Correlation between the carbon isotopic composition of planktonic foraminifera-bound organic matter and surface water pCO_2 across the equatorial Pacific

Keiran A. Swart [a,b*], Sergey Oleynik [a], Alfredo Martínez-García [b], Gerald H. Haug [b, c], Daniel M. Sigman [a]

[a] Department of Geosciences, Princeton University, Princeton, NJ 08540, USA.

[b] Department of Climate Geochemistry, Max Planck Institute for Chemistry, 55128 Mainz, Germany.

[c] Department of Earth Sciences, ETH Zürich, CH-8092 Zürich, Switzerland

*Corresponding Author.

E-mail Address: keiran@alumni.princeton.edu (K. Swart)

Telephone Number: 305 766 1693

Abstract

For times prior to those represented by the air trapped in Antarctic ice core records, the concentration of CO_2 in the atmosphere must be reconstructed using geochemical proxies. The $\delta^{13}C$ of particulate organic carbon (POC) produced in ocean surface waters has previously been observed to covary with the concentration of CO_2 in the water. Relative to bulk sedimentary organic carbon, the minute quantity of organic matter trapped within the shell walls of planktonic foraminifera, "foraminifera-bound organic matter" (FBOM), has the potential advantage of being protected from diagenetic alteration and contamination by allochthonous organic matter. Here, with new protocols and instrumentation, FBOM-$\delta^{13}C$ is investigated as a potential proxy for the aqueous CO_2 concentration ($[CO_{2(aq)}]$) and thus the partial pressure of CO_2 (pCO_2) in past surface waters. We achieve a full method precision of 0.4‰ (1SD) on sample sizes of 20 nanomole C by adding a cryofocus step, a helium sheath flow to the oxidation and reduction reactors, and other modifications to an elemental analyzer and by introducing new approaches to reduce contamination during sample preparation. FBOM-$\delta^{13}C$ was analyzed in core-top sediments from the eastern tropical Pacific that originate from across the equatorial maximum in surface water $[CO_{2(aq)}]$. FBOM-$\delta^{13}C$ is lower than predicted for marine phytoplankton, consistent with a substantial lipid component in FBOM. Anticorrelation is observed between FBOM-$\delta^{13}C$ and climatological $[CO_{2(aq)}]$; the relationship is statistically significant ($P < .05$) in mixed-species samples and in 4 out of 5 picked species. The slope of the FBOM-$\delta^{13}C$:$[CO_{2(aq)}]$ anticorrelation is equivalent to or greater than has been measured for the $\delta^{13}C$ of suspended POC in the surface ocean. Based on the few species analyzed in this study, endosymbiont-bearing and -barren species do not clearly differ from each other either in terms of their average value of FBOM-$\delta^{13}C$ or the strength of the FBOM-$\delta^{13}C$:$[CO_{2(aq)}]$

anticorrelation, despite the recognized importance of the photosynthetic endosymbionts as a source of organic carbon for the symbiotic species. Correcting for variations in the $\delta^{13}C$ of $CO_{2(aq)}$ and phytoplankton growth rate did not improve the significance of the FBOM-$\delta^{13}C$:$[CO_{2(aq)}]$ anticorrelation. The findings support the possibility that FBOM-$\delta^{13}C$ can be used as a paleoceanographic proxy for surface water $[CO_{2(aq)}]$ and thus atmospheric pCO_2.

1. Introduction

Global climate is strongly affected by the atmospheric concentration of CO_2. The current fossil fuel-driven increase in CO_2 is faster than any of its known variations over the last million years (Ruddiman, 2003; Zalasiewicz et al., 2008; Lüthi et al., 2008), with profound consequences for the global environment and human activities. Confident prediction of future climate change requires a more robust understanding of the processes controlling the concentration of CO_2 in the atmosphere and of the quantitative impact of CO_2 on climate. This may be pursued by studies of Earth's past climates, some of which are partial analogs for future climate states. Ice cores provide a direct record of atmospheric CO_2 for the last 800,000 years (Lüthi et al., 2008). For times prior to 800,000 years ago, the only window we currently have on atmospheric CO_2 levels is through geochemical proxies (Royer et al., 2004; Zachos et al., 2008; Beerling and Royer, 2011), with important exceptions (Higgins et al., 2015; Yan et al., 2019). These proxies are established by calibration either with modern environmental variation (i.e., in the case of significant surface water pCO_2 gradients) or using the ice core CO_2 record. Existing paleoproxies for atmospheric CO_2 concentration have substantial uncertainties, and disagreements among proxies tend to increase with geologic time. Examples of such

discrepancies include differences of 100 ppm throughout the middle Miocene (Greenop et al., 2014), 300 ppm in the Oligocene (Pagani et al., 1999; Pearson and Palmer, 2000), 1500 ppm in the Eocene, and 2000 ppm during the Eocene Hyperthermals (Zachos et al., 2008). Given these uncertainties and disagreements, there is strong motivation to develop additional CO_2 paleoproxies. The object of the present study is to investigate the $\delta^{13}C$ of organic matter bound within and protected by the walls of the calcite tests of foraminifera, with a focus on the possibility that it might serve as a tool for paleo-pCO_2 reconstruction.

1.1. Marine organic matter carbon isotopic composition and the concentration of dissolved CO_2

One long standing proxy for the concentration of CO_2 in air or dissolved in water is the stable isotopic composition of carbon in organic matter, or $\delta^{13}C_{org}$ ($\delta^{13}C = \{^{13}C/^{12}C_{sample}\}/\{^{13}C/^{12}C_{reference}\}$-1], where the reference is international standard Pee Dee Belemnite (PDB)). The $\delta^{13}C$ of suspended particulate organic matter ($\delta^{13}C_{SPOM}$) has been observed to be related to the concentration of dissolved CO_2 ($[CO_{2(aq)}]$) in ocean surface waters, according to the following equation (Rau et al., 1989):

$$\delta^{13}C_{SPOM} = -0.8 * [CO_{2(aq)}] - 12.6 \qquad \text{Eq. (1)}$$

Global variation in $\delta^{13}C_{SPOM}$ greatly exceeds the observed range in the $\delta^{13}C$ of dissolved inorganic carbon (DIC) (Rau et al., 1982). The observed variability in $\delta^{13}C_{SPOM}$ must be driven by variation in either the isotopic fractionation associated with photosynthesis or by post-fixation metabolism. Indeed, it has long been known that $\delta^{13}C_{org}$ of newly produced biomass is sensitive to the concentration of the CO_2 in the environment ($CO_{2(aq)}$ for aquatic photosynthesizers), with higher environmental CO_2 concentrations resulting in lower $\delta^{13}C_{org}$ (more negative relative to

PDB) (Farquhar et al., 1989; Popp et al., 1989; Rau et al., 1992; Hinga et al., 1994) (Fig. 1, left side). This is the basis for the use of $\delta^{13}C_{org}$ as a paleoproxy for surface water [$CO_{2(aq)}$] and thus atmospheric pCO_2.

1.2. Alkenone carbon isotopic composition

To provide robust information on past environmental conditions, a putative proxy must not be altered during its incorporation into the geologic record. The utility of bulk C_{org} in marine sediment is compromised both by the potential for admixture of terrigenous and other exogenous inputs (Jasper and Gagosian, 1989; Jasper et al., 1994) and by microbially-driven degradation and other diagenetic processes (Hatch and Leventhal, 1997; Freudenthal et al., 2001; Lehmann et al., 2002). To avoid such complications, the field has focused on the development of "compound-specific isotopic analysis" (CSIA) (Popp et al., 1989; Jasper and Hayes, 1990; Hayes, 1993). For pCO_2 reconstruction, CSIA has been applied widely to alkenones, long-chain ketones that are produced by prymnesiophyte algae for use in membrane lipids (Pagani, 2013). This approach screens out non-photosynthetic metabolic isotopic effects while having the other benefits of CSIA mentioned above (Bidigare et al., 1991). Moreover, alkenone production is limited to certain species of Prymnesiophyceae (Marlowe et al., 1984; Brassell, 2014), reducing the potential for isotopic changes in downcore records that derive from phytoplankton community changes in the surface ocean. Finally, the alkenones are widely used to reconstruct sea surface temperature (Brassell et al., 1986) (Prahl and Wakeham, 1987), presenting a rare opportunity to reconstruct two key environmental parameters from the same compounds in the sediment.

However, alkenones often occur at extremely low concentrations in marine sediments, especially below subtropical oligotrophic regions with low productivity, and yet these are the

114 regions where (i) surface pCO_2 best approximates equilibrium with the atmosphere and (ii) the
115 $\delta^{13}C$ of phytoplankton biomass is most likely to be directly relatable to the surface water
116 concentration of aqueous CO_2. Regions productive enough to reliably produce high sinking
117 fluxes of alkenones are likely characterized by rapid supply of nutrient-rich subsurface water to
118 the surface. These environments are far from optimal for the alkenone-based pCO_2 proxy for two
119 reasons. First, their surface $[CO_{2(aq)}]$ and $\delta^{13}C_{ce}$ often deviate substantially from atmosphere
120 equilibrium. Second, they are characterized by relatively weak anticorrelation between $\delta^{13}C_{org}$
121 $[CO_{2(aq)}]$ due to high and variable phytoplankton growth rates (François et al., 1993; Goericke
122 and Fry, 1994). Alkenones are also highly mobile and thus prone to resuspension and lateral
123 transport, which reduces confidence in the origin of alkenones extracted from sediment and
124 provides a lower limit on the scale of spatial and temporal resolution that can confidently be
125 obtained (Ohkouchi et al., 2002; Mollenhauer et al., 2003).

126 The carbon isotopic composition of organic matter trapped inside diatom frustules has
127 also been applied to determine phytoplankton $\delta^{13}C$ (Singer and Shemesh, 1995; Mejía et al.,
128 2017). One potential advantage of this technique is that the measurement can be performed in
129 diatoms of a constant frustule size, circumventing the potential effects of changes in cell size
130 over time. However, as with alkenones, the distribution of diatom microfossils in marine
131 sediments tends to limit this approach to regions where $[CO_{2(aq)}]$ and $\delta^{13}C_{ce}$ are not in
132 equilibrium with the atmosphere.

133 1.3. Foraminifera-bound organic matter

134 Foraminifera are cosmopolitan calcareous amoeboid protists with a well-established
135 fossil record extending back to the Mesozoic. Foraminiferal calcite $^{13}C/^{12}C$, $^{18}O/^{16}O$, and other
136 isotopic and elemental ratio proxies have been applied to reconstruct temperature, salinity,

nutrient concentration, pH, and other oceanic properties (Murray, 2001; Kucera, 2007). Foraminifera provide a single fossil type for the reconstruction of multiple environmental parameters and are broadly distributed. These considerations encourage the exploration of FBOM as an additional archive of paleoclimate information.

FBOM has a range of virtues as a substrate for isotopic reconstructions. It is interlaminated with layers of calcite (Spero, 1988) and protected from degradation on the seabed, as evidenced by the consistency between the amino acid composition of modern and 300 kyr old tests (Robbins and Brew, 1990). FBOM is also isolated from exogenous sources of organic matter (Schroeder, 1975).

The first work on FBOM-$\delta^{13}C$ was conducted with the goal of reconstructing surface water pCO_2 during the Paleocene Eocene Thermal Maximum (Stott, 1992) and since Last Glacial Maximum, respectively (Maslin et al., 1996; Maslin et al., 1997). These studies found reproducible organic $\delta^{13}C$ values, indicating that FBOM-$\delta^{13}C$ could be reliably measured. They also suggested that it could be used to reconstruct past surface water primary photosynthate $\delta^{13}C$. Using this approach, one surprising result was the finding that surface ocean pCO_2 decreased during the Paleocene Eocene Thermal Maximum, which was attributed either to reduced upwelling associated with diminished wind stress or a readjustment of carbonate equilibria (Stott, 1992). Recent work on FBOM has focused on its nitrogen isotopic composition ($\delta^{15}N$) (Ren et al., 2009; Ren et al., 2012). FBOM-$\delta^{15}N$ has been applied to paleoceanographic reconstructions of low latitude nitrogen fixation (Ren et al., 2009; Straub et al., 2013; Ren et al., 2017) and high latitude nitrate consumption (Straub et al., 2013; Martínez-García et al., 2014; Ren et al., 2015). The parallel analysis of FBOM-$\delta^{15}N$ and -$\delta^{13}C$ may further broaden the paleoceanographic utility of foraminifera tests (Pearson, 2012).

However, foraminifera are complex in terms of organic carbon source. By default, they are heterotrophs, apparently feeding at multiple trophic levels as well as consuming organic detritus in some cases (Bé et al., 1977). Moreover, many species have photosynthetic endosymbionts (Hemleben et al., 2012) (Fig. 1). Variability in external food sources is not an overwhelming concern, as $\delta^{13}C$ changes with trophic level are relatively minor (McCutchan et al., 2003). In contrast, the C isotopic effects of photosynthetic endosymbiosis are currently poorly known. The proportion of the organic carbon in symbiont-bearing foraminifera that derives from symbionts versus diet is uncertain. Microelectrode studies show that the net photosynthetic rate of the 'holobiont' (the collective host-symbiont system) is theoretically sufficient for the respiration and growth of the host (Jørgensen et al., 1985). As the symbionts are carried within the streaming cytoplasm of the foraminifera, the environment in which they fix organic carbon may not be representative of external conditions, and so the isotopic value of the carbon they provide to their hosts is uncertain. In the potentially analogous coral system, symbiont-bearing corals are shown to be significantly higher in $\delta^{13}C_{org}$ than both their diets (by ~4‰) and non-symbiont-bearing corals (by ~6‰) (Swart, 1983), suggesting the production of high $\delta^{13}C$ organic matter by the photosynthetic symbionts. The same sense of $\delta^{13}C_{org}$ difference is also seen in a comparison of two foraminifera species, one symbiont-bearing and the other not, but the offset is much smaller, 0.9‰ (Uhle et al., 1997). Seasonal studies of *Montastrea faveolata* show that the $\delta^{13}C_{org}$ of both zooxanthellae (symbiotic dinoflagellates) and host coral tissue fluctuates, with higher net fixation elevating the $\delta^{13}C_{org}$ (Fitt et al., 2000; Swart et al., 2005). The $\delta^{13}C$ values of both become most negative and the difference between them becomes the smallest in the summer months when the concentration of zooxanthellae is the lowest, a

situation consistent with the zooxanthellae as a source of relatively high $\delta^{13}C$ organic carbon to the 'holobiont.'

FBOM-$\delta^{13}C$ also may be influenced by fractionation associated with post-fixation formation of its constituent biomolecules (Abelson and Hoering, 1961) (DeNiro and Epstein, 1977), the biochemical composition of which has not yet been well-characterized. Prior studies have sought to characterize the foraminifera organic lining, a physically distinct material (Fhlaithearta et al., 2013) which may be chemically and isotopically distinct from the rest of the FBOM (e.g., the more diffusely distributed component). FBOM-$\delta^{13}C$ must thus be considered as potentially influenced by (1) the foraminifera's mechanisms of carbon acquisition (feeding and transfer from symbionts if present), (2) the internal carbon cycling of the 'holobiont,' and (3) the biosynthetic composition of FBOM incorporated into the test (Fig. 1, right side). The contributed fraction and isotopic composition of symbiont-derived carbon and its potential for fluctuation is, *a priori*, a central concern for the utility of FBOM-$\delta^{13}C$ as a proxy for surface water [$CO_{2(aq)}$]. Below, we investigate the significance of symbiont-derived carbon by comparison of FBOM-$\delta^{13}C$ in different foraminifera species.

1.4. Ground-truthing of FBOM-$\delta^{13}C$ as a proxy for surface ocean [$CO_{2(aq)}$]

In this study, we analyze multiple species of foraminifera from a suite of core tops (Table 2) taken from the eastern tropical Pacific across the equatorial upwelling zone. The region shows a strong, largely meridional [$CO_{2(aq)}$] gradient of ~200 µatm (Fig. 6), which should correspond to a $\delta^{13}C_{POM}$ gradient of ~5.6‰ (Rau et al., 1997), although surface water $\delta^{13}C_{SPOM}$ measurements in the region have shown a more muted response (Goericke and Fry, 1994). There are other environmental and biological gradients in the region that may also impact the $\delta^{13}C$ of newly produced photosynthate. A key consideration is phytoplankton growth rate (µ), which can vary

205 due to macronutrient concentration (Laws and Bannister, 1980), micronutrient concentration
206 (principally iron) (Sunda and Huntsman, 1997), or temperature (Eppley, 1972) in instances of
207 nutrient saturation. As growth rate increases, the intracellular $[CO_{2(aq)}]$ decreases and $\delta^{13}C$ may
208 become higher (Laws et al., 1995). Equatorial upwelling brings cold, high-nutrient and high-
209 $[CO_{2(aq)}]$ water of low $\delta^{13}C$ to the surface (Fig 5A/B), and so theoretically influences $\delta^{13}C_{org}$ in
210 two opposing ways, lowering $\delta^{13}C_{org}$ due to high $[CO_{2(aq)}]$ of low $\delta^{13}C$ but raising $\delta^{13}C_{org}$ due to
211 high growth rate. On the one hand, this complicates the attempted analysis because of the
212 inherent complexity of overlapping signals (CO_2 vs. μ). On the other hand, it provides an
213 effective test as to the relative importance of $[CO_{2(aq)}]$ *versus* growth rate in controlling FBOM-
214 $\delta^{13}C$.

215 ## 2. Methods

216 The following is an introductory summary of the entire analytical procedure. Each core top
217 sample is wet sieved at 120 μm, yielding a coarse fraction dominated by planktonic foraminifera.
218 In most cases, a subsample was then picked for individual planktonic species. The whole
219 foraminifera are cracked open and subjected to a chemical cleaning. Cleaned material is
220 pulverized, decanted into low-blank vessels, and decarbonated (Fig. 2). Samples are combusted
221 in a modified 'NanoEA' (Polissar et al., 2009), with the resulting CO_2 cryofocused and analyzed
222 by gas-source isotope ratio mass spectrometry (Fig. 3). In the following subsections, we describe
223 each step of the overall method, working backward from the combustion and isotopic analysis
224 system to the sample preparation.

225 ### 2.1. Instrument Design

Prior studies involving the measurement of FBOM-$\delta^{13}C$ (Stott, 1992; Maslin et al., 1996; Maslin et al., 1997) faced comparatively high sample size requirements (50 individual specimens per sample) and labor demands (manual extraction on a gas line). The current study employs instrument innovations that permit a new approach to these analyses. The entire system is described below, with innovations noted accordingly.

The sample is combusted through a Costech Elemental Combustion System (ECS 4010 CHNS-O) that has been extensively modified (Fig. 3, 'Combustion System'). The sample is introduced via a Costech 'Zero-Blank' autosampler (Costech, Valencia, CA, USA) (not depicted), which has been modified to be evacuated with a diaphragm pump and refilled with helium carrier gas from the continuous flow purging system, separated from the rest of the system with an isolation valve (Polissar et al., 2009).

The sample drops into a combustion reactor that has been modified to both reduce atmospheric CO_2 contamination and to concentrate analyte so as to allow for a shorter trapping time in the subsequent cryofocus, reducing instrumental blank. The reactor consists of concentrically housed quartz tubes. The outer tube is of the same diameter as the commercial system (14.8 mm inner diameter (i.d.), 18 mm outer diameter (o.d.)), and fixed to the instrument housing as in conventional instrumentation. The inner tube is 11 mm (i.d.) and 13 mm (o.d). and rests upon an internal hollow 'basal pin' that is welded to the base fitting and connected to a corresponding pin in the second reactor and is made flush with the inner tube by a combusted 'aluminum foil O-ring', which is sealed by tightening. Upon entering the instrument, the carrier gas bifurcates into a 'sample flow' which enters the inner tube and exits through the hollow basal pin, and a 'helium sheath' which flows through the space between the inner and outer tubes. These separate flows are carried over in corresponding positions into the chemical reduction

reactor via steel capillaries (0.5 mm i.d. for the helium sheath flow, 0.75 mm i.d. for sample flow). The reduction reactor is similarly divided into a sample-carrying central chamber for the sample flow and an external volume for the sheath flow. With the sample stream insulated in this way from direct points of contact with the atmosphere, we have reduced the instrumental blank to ~1 nmol C (~3 orders of magnitude lower than in conventional instrumentation), rendering it largely insensitive to trapping time.

The oxidative reagents typically used in the combustion reactor have been eliminated and replaced with a solid quartz rod (1 cm wide), resting on a section of 'wadded' silver wool (for halogen removal). This allows for the tube to be replaced and reused after each run without devitrification, and custom-built low-blank capsules are also reused (see below). The elimination of oxidative reagents also eliminates the tailing of the CO_2 sample pulse, which interferes with complete sample trapping and can also lead to sample 'carry-over,' the contamination of a sample by previous samples. The interior tube is fluted to minimize the conduction of heat through the central rod to the pin at the base, and the bottom connectors are cooled by a fan to prevent thermal degradation of the rubber o-rings affixing the exterior tubes to the instrument housing at the thermal collar. The reduction reactor is constructed similarly, with a solid copper rod spanning the length of the hot zone of the reactor, bracketed by quartz rods to reduce dead volumes and the conduction of heat. The combustion chamber temperature is held at 1000°C, the reduction at 650°C. The flow from the central chamber passes through a tube for water trapping (4mm i.d., 6mm o.d.) that is filled with Sicapent® (phosphoric pentoxide drying agent), and the flow bypasses the on-board gas chromatographic tube and thermal conductivity detector. The helium sheath is vented to waste after the reduction reactor. The sample flow rate was reduced from the standard 100 ml/min to 40 ml/min (to better trap the analyte cryogenically), controlled

by the EA mounted pressure regulator, while the helium sheath flow rate is at 15 ml/min, controlled by a manually adjusted crimp constricting the diameter of the helium sheath exhaust.

The modified Elemental Analyzer (EA) and the Isotope Ratio Mass Spectrometer (IRMS) interface with a repurposed Finnigan Gasbench II to cryofocus the analyte (bottom of Fig. 3 marked 'cryofocus') (Casciotti et al., 2002). Sample flow enters the cryofocus trap through 0.45mm i.d. silica capillary into a 1 m long, 2 mm i.d., doubly looped stainless-steel capillary in which the sample CO_2 is frozen out of the helium carrier flow by immersion in liquid N_2; the loop is lowered by piston to be immersed from the beginning of the sample combustion step. In 'Load' mode, the sample-containing helium flow from the EA passes through the trap, after which the carrier gas vents to waste. During this step, the rest of the system is plumbed with helium carrier at 'low-flow' (2 ml/min). Once the sample is trapped, a pneumatically operated 6-port Valco valve switches to 'Inject' mode, and the looped stainless-steel capillary is carried upward by the piston out of the liquid N_2 bath. 'Inject' mode connects the tail end of the of the sample collection loop to the low-flow helium while the high-flow helium carrier from the EA bypasses the trap and vents to waste. The low-flow helium and entrained CO_2 passes through a 'PoraPLOT Q' fused silica cap gas chromatographic column (25 m long, 0.32 mm i.d.) and a Nafion® dryer, towards an open split, through which it proceeds at 0.2 ml/min through a 0.1 mm i.d. silica capillary to a Thermo Delta V Plus isotope ratio mass spectrometer.

2.2. Sample Preparation

Surface sediment was obtained from a suite of core tops (0-3 cm from surface) across the equatorial Pacific ranging between 14°S and 5°N and 105°W and 85°W (Table 2). Sediments are wet sieved at >120 μm, and unpicked, mixed-species planktonic foraminifera are set aside as one aliquot. The largest component of the mixed species fraction, both by number of individuals and

295 mass, was *Globorotalia menardii*. From the remaining sieved material, individual foraminifera
296 species are picked for analysis. Below, we describe the species in terms of two groups: 1) shallow-
297 dwelling, obligatorily symbiotic, dinoflagellate-associated foraminifera ("symbiotic" species):
298 *Orbulina universa* and *Globigerinoides sacculifer,* and (2) deeper-dwelling species with
299 facultative chrysophyte associations ("facultative" species): *Globorotalia menardii, Globigerina*
300 *dutertrei,* and *Puleniatina obliquiloculata*. The tests are cracked open (but not pulverized) under
301 a microscope using a watch glass lens and then transferred to 4 ml silanized (silica coated) glass
302 vials that were previously combusted at 500 ^{o}C in a muffle furnace (Fig. 2, box 1). The vials are
303 sealed with polypropylene caps with microwave-bonded PTFE septa; these were precleaned first
304 in ethanol and then in high purity water.
305 To remove clays, samples are ultrasonicated for 15 minutes in 4 ml of 2% sodium
306 polyphosphate that has been buffered to a pH of 8 with NaOH; the supernatant is then removed
307 with a vacuum aspirator. The sample is resuspended in deionized water and vortexed, and these
308 steps are repeated twice more (Fig. 2, box 2). To remove metal oxide coatings, the samples
309 undergo a reductive cleaning with sodium bicarbonate-buffered dithionite-citrate (pH 7) in an 80
310 ^{o}C water bath (Mehra and Jackson, 2013) and are rinsed as previously. The samples undergo an
311 oxidative cleaning consisting of autoclaving for 120 minutes at 122 ^{o}C in a potassium persulfate
312 and sodium hydroxide solution (Ren et al., 2009; Ren et al., 2012). The samples are then rinsed
313 as before, dried, and pulverized with a combusted glass rod for better homogenization
314 (pulverization is conducted after the oxidative cleaning to avoid powder loss during the cleaning)
315 (Fig. 2, box 3).
316 The last preparative step is decarbonation to remove the mineral phase of the shell that
317 would otherwise interfere with the measurement of the FBOM. This is conducted by acid

318 dissolution in the sample vial, with no subsequent decanting of either spent solution or sample,
319 to ensure retention of the entire FBOM sample. In initial efforts, cleaned sample was packed into
320 silver capsules as often used in total carbon analysis and previously developed NanoEA protocols
321 (Wooller et al., 2008; Polissar et al., 2009). However, these were found to make a high and
322 variable contribution to the blank, regardless of cleaning approaches. Precombustion of the silver
323 capsules reduced their structural integrity, causing them to leak acid during decarbonation and to
324 tear readily during packaging. Instead, samples are dissolved in quartz capsules that are cut from
325 4 mm (o.d.) tubing (sealed with a torch and the base flattened) and positioned on a purpose-built
326 ceramic well plate (Macor), using ceramic tipped tweezers (both combusted). Approximately 0.2
327 mg of cleaned crushed foraminiferal carbonate is aliquoted into each capsule. Samples are then
328 submerged in high purity water before being dissolved in net 1N HCl; this prevents the
329 effervescence associated with decarbonation from inhibiting contact of sample grains with the
330 solution. These samples are then dried in a vacuum-assisted oven, reacidified, and dried again for
331 12 hours (Fig. 2, box 3).

332 Individual analyses are corrected with a two-point calibration using internationally
333 accepted reference materials USGS40 (glutamic acid, with a $\delta^{13}C$ of -26.39‰ *vs.* PDB) and
334 USGS65 (glycine, with a $\delta^{13}C$ of -20.29‰ *vs.* PDB). In their preparation, the aliquots of reference
335 material were acidified and then dried as for the samples. Sample analyses were repeated in
336 triplicate within 'batches' (samples grouped for sequential analyses on the NanoEA). In addition,
337 samples were measured across separate cleaning batches. A full methodological precision of
338 ±0.4‰ (1σ) against Vienna Pee Dee Belemnite (V-PDB) is observed across cleaning batches,
339 which is consistent with results from in-house coral standards.

340 The $\delta^{18}O$ and $\delta^{13}C$ of the mixed foraminiferal carbonate (Table 2), was measured to test
341 for consistency with Holocene (i.e. roughly modern) conditions. The foraminiferal carbonate was
342 converted to CO_2 with 103% phosphoric acid using an automated Kiel III device at the University
343 of Miami. Mass isotopologues of carbon dioxide (44-46) were measured using a Thermo Delta
344 Plus and were corrected to $\delta^{13}C$ and $\delta^{18}O$ values (Craig, 1957), modified for a triple collector mass
345 spectrometer. Precision was ±0.08‰ (1σ) VPDB for oxygen and ±0.03‰ (1σ) VPDB for carbon.
346 2.3. Ancillary properties
347 Surface water [$CO_{2(aq)}$] concentrations are calculated based on surface ocean CO_2 fugacity
348 (fCO_2) and temperature from the Surface Ocean CO_2 Atlas (SOCAT) (Bakker et al., 2016), using
349 the Henry's Law constant for the solubility of CO_2 in seawater from (Zeebe and Wolf-Gladrow,
350 2001).
351 We explored the role of spatial patterns in phytoplankton growth rate in explaining the
352 FBOM-$\delta^{13}C$ data. Growth rate (μ, in units of divisions per day) was calculated from remote sensing
353 data using the pertinent expressions of (Behrenfeld et al., 2005):
354 $\mu = 2 * \text{Chl:}C_{sat}/[0.022 + (.045 - .022)exp^{-3Ig}] * (1 - exp^{-3Ig})$ Eq. (2)
355 where Chl:C is the ratio of phytoplankton chlorophyll to carbon biomass, and I_g is the monthly
356 median mixed layer light level. Chl:C_{sat} can be estimated by applying a scalar to particulate
357 backscatter coefficient $b_{bp}430$ (AquaMODIS GIOP model)(Werdell et al., 2013) with Chl data
358 sourced from (Hu et al., 2012).
359 $C = 13000 \text{ x } (b_{bp}430 - .00035)$ Eq. (3)
360 I_g can be determined by the following equation:
361 $I_g = I_0 exp^{-k490*MLD/S}$ Eq. (4)

where I_0 is cloud-corrected surface PAR (SeaWiFS data; (Frouin et al., 1989), MLD is mixed layer depth (CMIP5 NOAA GFDL-CM2.1, (Taylor et al., 2012)), and k490 (SeaWiFS data; NASA/GSFC/OBPG) is the mixed layer light attenuation coefficient at 490 nm wavelength.

3. Results

3.1. Foraminiferal carbonate $\delta^{18}O$

For comparison of coretop FBOM-$\delta^{13}C$ with modern [$CO_{2(aq)}$] or other modern properties to be valid, as a minimum requirement, the foraminifera must be of Holocene age as opposed to deriving from the last deglaciation or some prior time. In order to test this, we measured the $\delta^{18}O$ of the mixed species foraminiferal carbonate ($\delta^{18}O_{carb}$) (Fig 4, EA1, Table 2). Across analyzed stations, $\delta^{18}O_{carb}$ varies between 0.05 and -1.59‰ vs. PDB, with the exception of an outlier at site 6.52°S and 103.25°W, with a value of 1.54‰. The mean $\delta^{18}O$ is -0.82‰ (or -0.92‰ when excluding the outlier).

Given modern conditions, the $\delta^{18}O$ of surface seawater ($\delta^{18}O_{sw}$) is estimated to vary from 0.58 to -0.09 across the sites (Schmidt, 1999). At each sample site, based on depth variation of $\delta^{18}O_{sw}$ and temperature and using existing empirical calibrations, we calculate the $\delta^{18}O$ of foraminiferal carbonate as a function of depth for the symbiotic *G. sacculifer* (Erez and Luz, 1983) and *O. universa* (Bemis et al., 1998) (Fig. 4, EA1). These species are both major components of our mixed-species samples. Given the 'low-light' *O. universa* calibration, the average measured $\delta^{18}O_{carb}$ at our sites yields a temperature roughly 3°C cooler than is observed at the surface across the sites. The most likely explanation for the discrepancy with surface-calculated $\delta^{18}O_{carb}$ is that the constituent foraminifera calcified at depth. If we compare the range of habitats of our constituent foraminifera species (Fig. 4, right side), we can demonstrate the

likely overlap in the depth of habitat of the principal components of the mixed species fraction. The most abundant of the mixed species by mass is *G. menardii* (likely followed by O. *universa* and *P. obliquiloculata),* whose range overlaps those of the more shallowly dwelling surface foraminifera at around 50 m water depth (Fairbanks et al., 1982; Faul et al., 2000). Taking into account both the lower temperature and the higher $\delta^{18}O_{sw}$ at depth (Ford et al., 2018), the $\delta^{18}O_{carb}$ data can be explained with a calcification depth range of ~30-75 m (Fig. 4, EA1). Thus, for reasonable assumptions about calcification depth, the $\delta^{18}O$ data appear consistent with a Holocene age for the preponderance of the core top samples. However, given the potential effects from the depth of calcification and other factors, we cannot rule out a contribution from deglacial- or glacial-age foraminifera. For example, if all calcite precipitation were assumed to occur at the surface, the measured mean $\delta^{18}O_{carb}$ would be roughly consistent with high-light *O. universa* formed in a glacial ocean that was ~1‰ higher in $\delta^{18}O_{sw}$ (Schrag et al., 2002) and 2.6°C colder (Lea et al., 2000).

We can also compare our $\delta^{18}O_{carb}$ measurements to the analysis of eastern equatorial Pacific core-tops that had been verified as Holocene by radiocarbon dating (Faul et al., 2000). The latter study observed mean $\delta^{18}O_{carb}$ of -1.6‰ for *G.sacculifer,* -0.3‰ for *O.universa* and -0.1‰ for *G. menardii*. The mean value of our measurements mixed-species $\delta^{18}O_{carb}$ is intermediate among these species, consistent with our core-tops representing Holocene conditions. Furthermore, regional sedimentation rates for our core sites were interpolated from a compilation of prior measurements (Table 2) and vary from 1.8 to 5.4 cm/kyr. Given these sedimentation rates, no core-site sample depth would confer an age greater than 7.7 kyr ago.

3.2. Foraminifera-bound organic matter $\delta^{13}C$

The use of $\delta^{13}C_{org}$ as a tool to reconstruct past $[CO_{2(aq)}]$ is through the net isotope effect of photosynthetic biomass production, ε_p, which is calculated from $\delta^{13}C_{org}$ and the $\delta^{13}C$ of $CO_{2(aq)}$:

$$\varepsilon_p = ([(\delta^{13}C_{org} + 1000)/(\delta^{13}C_{CO_2} + 1000)] - 1)1000 \quad \text{Eq. (5)}$$

$\delta^{13}C_{CO2}$ (Fig. 5B), is often estimated from the $\delta^{13}C$ of cooccurring foraminiferal carbonate (Table 2) and laboratory-derived, temperature dependent isotope effects (Mook, 1986; Zhang et al., 1995) to account for the equilibrium fractionations among the species of dissolved inorganic carbon.

$$\delta^{13}C_{CO2} = \delta^{13}C_{[CO_3{}^{2-}]} - \varepsilon_{cb} - (1 + \varepsilon_{db} * 10^{-3}) + \varepsilon_{db} \quad \text{Eq. (6)}$$

where CO_3^{2-} refers to carbonate, ε_{cb} refers to the fractionation between carbonate and bicarbonate and equals (-867/T+2.52), and ε_{db} refers to the fractionation between $CO_{2(aq)}$ and bicarbonate and equals (-9866/T+24.12) (Mook, 1986).

Here, instead of ε_p, we report ε_{FBOM}, defined as follows:

$$\varepsilon_{FBOM} = ([(\delta^{13}C_{FBOM} + 1000)/(\delta^{13}C_{CO_2} + 1000)] - 1)1000 \quad \text{Eq. (7)}$$

Culture and modern ocean studies will be required to relate ε_{FBOM} to ε_p. ε_{FBOM} is a measure of the $\delta^{13}C$ difference between the biomineral trapped organic C of a heterotrophic organism (foraminifera) that feeds on heterotrophic and autotrophic prey and hosts autotrophic endosymbionts. Thus, its interpretation is potentially more nuanced than that of ε_p from an autotrophic source, such as in the case of alkenones from prymnesiophytes.

Mixed species FBOM-$\delta^{13}C$ varies between -25.59 and -29.13‰ (Fig. 5C), with a mean value of -27.35‰ (Fig. 5C, 7A, Table 1). Mixed species ε_{FBOM} varies between -16.54 and -

20.44‰, with a mean value of -18.48‰, and an even distribution between end members (Fig. 5D, 7D, Table 1). The aforementioned outlier in $\delta^{18}O$ is not associated with a concomitant outlier in $\delta^{18}C$. Among the symbiotic species, the FBOM-$\delta^{13}C$ of *O. universa* varies between -23.80 and -29.18‰, with a mean value of -26.55‰ (Fig 5C, 7B, Table 1). *G. sacculifer* varies between -23.58 and -29.93‰, with a mean value of –26.43‰. Its range is the greatest amongst the picked species, ~50% greater than that of the mixed species fraction, attributable to a ~1.8‰ higher maximum value. ε_{FBOM} shows no patterns that are distinct from those of FBOM-$\delta^{13}C$. The ε_{FBOM} of *O. universa* varies between -14.27 and -19.81‰, with a mean value of -17.72‰ (Fig 5D, 7E, Table 1). *G. sacculifer* varies between -14.14 and -21.10‰, with a mean value of –17.81‰. The mean values for the symbiotic species are within 0.09‰ of each other.

The second group is the deeper dwelling species with potential facultative symbioses with chrysophyte algae: *G. menardii, G. dutertrei,* and *P. obliquiloculata*. For FBOM-$\delta^{13}C$, *G. menardii* varies between -23.44 and -29.13‰, with a mean value of -26.8‰ (Fig. 5C, 7C, Table 1); *G. dutertrei* varies between -24.20 and -28.69‰, with a mean value of –26.59‰; and *P. obliquiloculata* varies between -24.23 and -28.14‰, with a mean value of –26.24‰. The chrysophyte-associated foraminifera do not share any consistent similarities with each other compared with the other picked species. *G. dutertrei* and *P. obliquiloculata* are the most similar among picked species, showing the least variation overall, with lower maximum and higher minimum $\delta^{13}C$ (ranges are 10% and 20% greater than that of the mixed species samples). In contrast, *G. menardii* has an absolute range more closely matching the dinoflagellate-associated species (5.69‰ compared with 5.30‰ for *O.universa* and 6.35‰ for *G.sacculifer*). As in the dinoflagellate-associated foraminifera, ε_{FBOM} shows no patterns distinct from FBOM-$\delta^{13}C$. For ε_{FBOM}, *G. menardii* varies between -14.66 and -20.29‰ (Fig. 5D, 7C, Table 1), with a mean

450 value of -18.00‰. *G. dutertrei* varies between -15.48 and -20.24‰, with a mean value of –
451 17.79‰. *P. obliquiloculata* varies between -14.63 and -19.86‰, with a mean value at –17.37‰.

452 It is noteworthy that the FBOM-$\delta^{13}C$ and ε_{FBOM} of the mixed species fraction are on
453 average more negative than any of the sampled species (Fig.5C, Table 1). Mixed species ε_{FBOM} is
454 on average -0.48‰ more negative than its closest measured component (*G. menardii*), an offset
455 equivalent to the maximum difference between measured species (-0.63‰ between *P.*
456 *obliquiloculata* and *G. menardii*). However, this is largely attributable to three sample sites, with
457 the median FBOM-$\delta^{13}C$ of the mixed species fraction more closely matching that of the picked
458 species. The mixed species assemblage also shows less variation than any of the picked species.

459 The carbon concentration of mixed species FBOM ranges between 66 and 112 µmol C/g
460 of carbonate (0.08-0.14 wt%), with a mean of 82 µmol C/g (~0.1 wt%). *O. universa* ranges
461 between 72 and 118 µmol C/g (0.09-0.14 wt%), with a mean of 87 µmol C/g (0.11 wt%). *G.*
462 *sacculifer* varies between 61 and 111 µmol C/g (0.07-0.13 wt%), with a mean of 82 µmol C/g
463 (0.1 wt%). *G. menardii* ranges between 60 and 101 µmol C/g (0.07-0.12 wt%), with a mean of
464 82 µmol C/g (0.09 wt%). *G. dutertrei* varies between 60 and 109 µmol C/g (0.07-0.13 wt%),
465 with a mean of 83 µmol C/g (0.1 wt%). *P. obliquiloculata* varies between 53 and 109 µmol C/g
466 (0.06-0.13 wt%), with a mean of 82 µmol C/g (0.1 wt%). There is no clear distinction in the
467 carbon content between the picked groups, among picked species, or between the picked groups
468 and the mixed species samples. These concentrations are all higher than are observed in coral
469 skeleton-bound organic carbon, of ~30 µmol C/g (Ingalls et al., 2003) (our in-house coral
470 standard yielding a long term average of ~42.6 ±4.2 µmol/g).

471 3.3. Spatial variation

The FBOM-$\delta^{13}C$ and ε_{FBOM} of both mixed and picked species show strong and consistent variation with latitude (Fig. 5C/D, 6). Most species are at their minimum ε_{FBOM} between 0 and 5°S of the equator, rising steeply at higher latitudes (Fig. 5C, 6, A2). The ε_{FBOM} minimum between 0 and 5°S is co-located with the zone of equatorial upwelling, which is characterized by the exposure of cold, CO_2-rich water (Fig. 5A, 6, A2). The exception is *P. obliquiloculata*, which displays a negative outlier at 1.25°N, but otherwise follows the same pattern. Most picked species overlap with the mixed foraminifera fraction between 6.51°S and 1.25°N but decouple to the North and South of this range (Fig. 5D). Most of the sample sites occur along a meridional transect along 103°W (Fig. 6, EA2). Variation in ε_{FBOM} along this transect exceeds any zonal variation seen, excepting sites that also exceed the latitude range of the main transect (Fig. 6, EA2). As such, longitude appears to have a weak impact on ε_{FBOM}, with no statistically significant variation ($P > .05$) for any species fraction.

3.4. Anticorrelation with $[CO_{2(aq)}]$

When plotted against latitude, ε_{FBOM} and the surface water $[CO_{2(aq)}]$ are in antiphase (Fig. 5A/D). This suggests that variation in $[CO_{2(aq)}]$ is the underlying cause of the variation of ε_{FBOM} with latitude. When the ε_{FBOM} of the mixed foraminifera fraction is plotted against $[CO_{2(aq)}]$ concentration, there is significant anticorrelation (slope: -0.37, R: 0.5, $P < .05$, n = 23) (Fig. 7D, Table 1). Significant anticorrelation is also seen for each picked species excepting *P. obliquiloculata*; in each instance, the slope of the anticorrelation scales with the degree to which the data are predicted by the linear model (i.e., the R value). The dinoflagellate-associated species *G. sacculifer* (slope: -1.64, R: 0.84, $P < .01$, n = 8) and *O. universa* (slope: -1.06, R: 0.80, $P < .01$, n = 9) show the strongest anticorrelation with $[CO_{2(aq)}]$ (Fig. 7E, Table 1). This is

494 followed in order by *G. mendardii* (slope: -0.78, R: 0.69, P <01, n = 15) and *G. dutertrei* (slope:
495 -0.60, R: 0.60, P < . 05, n = 15) (Fig. 7F, Table 1). *G. dutertrei* is the closest to approximating
496 the slope observed in modern phytoplankton (Rau et al., 1992). The only species that shows
497 weaker anticorrelation with [$CO_{2(aq)}$] than the mixed species fraction is *P. obliquiloculata* (slope:
498 -0.36, R 0.32, P > . 05, n =11). Similar anticorrelations are observed for FBOM-$\delta^{13}C$ with
499 [$CO_{2(aq)}$] (Fig. 7; Table 1); correlation coefficients are slightly stronger, suggesting that the use of
500 foraminiferal carbonate $\delta^{13}C$ to reconstruct $\delta^{13}C_{CO2}$ introduces additional error.

501 4. Discussion

502 The discussion below focuses on three key observations. First, the average values of
503 FBOM-$\delta^{13}C$, whether considering individual species or mixed foraminifera, are notably lower
504 than the $\delta^{13}C$ of suspended and sinking organic matter in the tropical Pacific, consistent with
505 measurements of FBOM-$\delta^{13}C$ in the literature (Stott, 1992; Maslin et al., 1996; Maslin et al.,
506 1997). We propose to explain this observation in terms of the chemical composition of FBOM.
507 Second, ε_{FBOM} is observed to vary inversely with [$CO_{2(aq)}$], with a similar strength of
508 dependence as is observed on a global ocean basis for $\delta^{13}C_{SPOM}$. This finding was the anticipated
509 outcome, and it bodes well for the utility of ε_{FBOM} as a tool for reconstruction of surface water
510 [$CO_{2(aq)}$] and thus atmospheric CO_2 in the past. Third, findings that were not anticipated are that
511 the ε_{FBOM} of spinose, dinoflagellate-bearing symbiont foraminifera had similar average values
512 and showed a similar relationship with [$CO_{2(aq)}$] as the non-spinose foraminifera that are believed
513 to rely less on endosymbiont photosynthesis. This result, while potentially beneficial for proxy
514 application, was unanticipated because the $\delta^{13}C_{org}$ of dinoflagellate-bearing scleractinian corals is
515 higher than that of its prey (Goreau, 1977; Swart, 1983), with preliminary evidence from a

culture study for a similar effect of dinoflagellate symbiosis in planktonic foraminifera (Uhle et al., 1997) (see section 1.3). We consider the behavior and physiology of foraminifera and their likely impacts on the $\delta^{13}C$ of foraminiferal biomass and thus on ε_{FBOM}, proposing possible explanations for the broad similarity in both the absolute values and the anticorrelations with $[CO_{2(aq)}]$ across the different picked species measured in this study.

4.1. Dynamics of marine POM-$\delta^{13}C$

In order to interpret the significance of measured ε_{FBOM}, it must first be put in the context of the expected and observed $\delta^{13}C$ of organic carbon in the upper ocean, upon which foraminifera feed. The $\delta^{13}C_{SPOM}$ of low latitude surface Pacific is observed to fall mostly between -22 and -18‰ (Rau et al., 1992; Goericke and Fry, 1994). Given the high $[CO_{2(aq)}]$ associated with equatorial upwelling (Bates et al., 1993), together with evidence from both field studies and phytoplankton cultures on its expected effect on ε_p (Rau et al., 1992; Burkhardt et al., 1999), a $\delta^{13}C_{SPOM}$ minimum of -22‰ would be expected in the eastern equatorial Pacific; however, as yet, to our knowledge, no such feature has been documented (Degens et al., 1968). According to our calculations based on satellite-derived phytoplankton growth rates (Fig. 8, Table 1), (see below), spatial variation in growth rate cannot explain the lack of a $\delta^{13}C_{SPOM}$ minimum. Spatial variation in the penetration of anthropogenic CO_2 into the upper ocean may play a role in this discrepancy (Chen et al., 2006). $\delta^{13}C_{SPOM}$ has also been shown to covary with SST, with estimates ranging from 0.12-0.31‰ per °C (Goericke and Fry, 1994); this may in part be due to the temperature dependence of the $\delta^{13}C$ difference between atmospheric and aqueous CO_2 at equilibrium, which is approximately 0.12‰ per °C (Mook et al., 1974). However, such a temperature dependence would not explain the existence of the equatorial minimum in FBOM-$\delta^{13}C$ but its absence in $\delta^{13}C_{SPOM}$.

Two depth profiles of $\delta^{13}C_{SPOM}$ at 2°S, 140°W and 12°S, 135°W show a decline of ~3‰ from the surface mixed layer to 100-200 m depth but show divergent patterns at greater depth (Benner et al., 1997). In general, $\delta^{13}C_{SPOM}$ displays substantial variation with depth, typically decreasing by 2-5‰ down to 200 m (Druffel et al., 1992) but then increasing at greater depths (Eadie and Jeffrey, 1973).

The $\delta^{13}C$ of sinking POM in the upper water column tends to parallel spatial variation in the $\delta^{13}C_{SPOM}$ in the euphotic zone, although with a negative offset (Rau et al., 1992) that tends to increase with depth (Nakatsuka et al., 1997). Processes modifying sinking POM are not well constrained (Hwang et al., 2004); sinking particles are thought to interact both with SPOM (physically and through biological aggregates) and DOM (by sorption-desorption) (Smith et al., 1992; Druffel et al., 1992). Its low $\delta^{13}C$ has been proposed to result from the selective decomposition of ^{13}C-rich components such as carbohydrates and amino acids, which are particularly susceptible to microbial degradation (Benner et al., 1997). This is supported by incubation experiments, which find relative enrichment of lipids in residual POM undergoing decay (Harvey et al., 1995)(Lehmann et al., 2002). It is less likely that this ^{13}C depletion is the result of the addition of some new low-$\delta^{13}C$ material; bacteria tend to be higher in $\delta^{13}C$ than the substrate on which they are feeding (Macko and Estep, 1984). Preferential preservation of terrestrial organic matter in the sinking flux may be important in some settings, thus lowering the $\delta^{13}C$ of sinking POM, but this is unlikely to be a significant effect in the open equatorial Pacific.

4.2. Low $\delta^{13}C$ of FBOM in comparison to marine POM

Despite the endosymbiotic photosynthesizers in some species, planktonic foraminifera are fundamentally a heterotrophic organism (Anderson et al., 1979). Thus, a starting point for interpretation of ε_{FBOM} is its comparison to that of POM available in its environment. The $\delta^{13}C$

change per trophic level in zooplankton is modest, varying between -0.1 through 0.4‰ (McCutchan et al., 2003), and so foraminiferal bulk biomass $\delta^{13}C$ should broadly match diet or perhaps be slightly (≤1‰) higher (DeNiro and Epstein, 1977). In contrast, we observe FBOM-$\delta^{13}C$ to be substantially lower than the mean equatorial Pacific $\delta^{13}C_{SPOM}$, by ~7.3‰ in the case of mixed foraminifera and ~6.5‰ in the case of picked species.

A culture study previously identified a more modest ^{13}C depletion of foraminiferal material relative to diet (Uhle et al., 1997). When fed a diet of *Artemis nauplii* with a $\delta^{13}C$ of -15.5‰, symbiont-bearing *O.universa* and asymbiotic *Globierina bulloides* were measured to have a biomass $\delta^{13}C$ of -17.4‰, and -18.5‰, respectively. The specific material measured by Uhle et al. was the portion of foraminiferal material that was captured on a filter (most likely a glass fiber filter with nominal pore size of 0.7 μm) after acidification; this material likely consists of biomass and shell-bound organic matter that is membrane-rich and thus not solubilized during the acidification. They thus attributed the ^{13}C depletion of both species relative to diet to a large proportional contribution from lipid, which tends to be 3-4‰ lower in $\delta^{13}C$ than the whole organism (Galimov, 2012). Similarly, alkenones (which are lipids) are observed to have a $\delta^{13}C$ that is 4.2‰ lower than prymnesiophyte biomass (Popp et al., 1998). A study that compared the $\delta^{13}C$ of phytoplankton off the west coast of Galapagos with that of $CHCl_3$-extracted lipids from the same material (Degens et al., 1968) found an isotopic offset of 10.5‰, with the lipids having a mean value of -29.8 ‰, interestingly similar to an FBOM-$\delta^{13}C$ of -28.5‰ at our nearby coretop.

Given this prior work, we suggest that the low $\delta^{13}C$ of FBOM is an indication of a high lipid content in this material. Consistent with this interpretation, the N content of FBOM from the tropical Pacific is 4-5 nmol N/mg (0.006-0.0075%) (Ren et al., 2017) for material with an

585 average C content of 90 nmol C/mg (±20.55 nmol C/mg), yielding a relatively high C:N ratio of
586 roughly 20. The ^{13}C depletion of FBOM relative to the expected foraminiferal diet coupled with
587 its high C:N ratio argue for a substantial lipid component (DeNiro and Epstein, 1977; Geider and
588 La Roche, 2002; Barnes et al., 2007).

589 To date, studies of the chemical composition of FBOM have focused on its amino acid
590 composition (King and Hare, 1972; Stathoplos and Hare, 1989), as opposed to its bulk chemical
591 composition. The possible structural contributors appear to be the outer organic layer and the
592 primary organic membrane, which are sequestered within the test (Allan W. H. Bé et al., 1979),
593 and some portion of the cytoplasmic envelope (involved in chamber formation). Acid dissolution
594 of two benthic species *A. lobifera* and *A.hemprichii* yielded two fractions of organic material:
595 "residual" organic matter (ROM) that remains in the particulate phase and acid-soluble organic
596 matter (ASOM) (ten Kuile and Erez, 1987). While ASOM was shown to be composed mainly of
597 low molecular weight compounds, the ROM consisted mainly of lipids in the case of *A. lobifera*
598 and of proteins and lipids in the case of *A.hemprichii*. Lipids in FBOM may stem from the
599 cytoplasm; lipids are dispersed throughout the cytoplasm, playing a role in foraminifers' active
600 vertical migration (Schiebel and Hemleben, 2017). It is more likely, however, that this
601 chemically distinctive material is encapsulated within the tests at the time of chamber formation
602 as the basis for the organic template for calcite nucleation (Schiebel and Hemleben, 2017).

603 4.3. Anticorrelation of ε_{FBOM} with $[CO_{2(aq)}]$

604 An idealized model of a phytoplankton cell has been used to predict ε_p under various CO_{2aq}
605 concentrations (Francois et al., 1993; Rau et al., 1997).

606 $$\varepsilon_p = \varepsilon_t + C_i/C_e * (\varepsilon_f - \varepsilon_t) \quad \text{Eq. (8)}$$

607 Where ε_t is the isotope effect associated with diffusion, ε_f with fixation, and C_i/C_e the ratio
608 between intra- and extra-cellular CO_2. According to this model, phytoplankton growth rate, cell
609 size, and cell shape can all affect ε_p, a conclusion supported by abundant culture data (Goericke
610 et al., 1994; Laws et al., 1995; Popp et al., 1998).

611 Since the proposal of this CO_2 diffusion-based model, evidence has arisen that these
612 phytoplankton characteristics have changed over glacial cycles, complicating the relationship of
613 ε_p to $[CO_{2(aq)}]$ (Zhang et al., 2019; Stoll et al., 2019). Moreover, the $\delta^{13}C$ of newly produced
614 photosynthate may often reflect additional processes (Wilkes and Pearson, 2019). These are
615 mostly related to carbon-concentrating mechanisms (Hopkinson et al., 2011), including the
616 active uptake of HCO_3^- (Keller and Morel, 1999; Cassar et al., 2004), especially at low $[CO_{2(aq)}]$
617 (Laws et al., 2002; Stoll et al., 2019) (Fig. 1). For example, recent work indicates that the
618 multiple steps by which CO_2 is interconverted with HCO_3^- and transported to RubisCO can
619 induce substantial net isotopic fractionation by photosynthesis under certain conditions, e.g.,
620 excess photon flux (Wilkes and Pearson, 2019).

621 Despite the diverse physiological controls on ε_p demonstrated in culture and in vitro, a
622 roughly linear anticorrelation between $\delta^{13}C_{SPOM}$ and $[CO_{2(aq)}]$ has been observed consistently in
623 modern surface waters (Rau et al., 1989; Goericke and Fry, 1994). Moreover, assuming such a
624 linear anticorrelation, $\delta^{13}C_{org}$ measurements in some deep sea sediment cores have roughly
625 replicated the ~80 µatm increase in atmospheric CO_2 across the last glacial/interglacial transition
626 (Jasper and Hayes, 1987)(Rau et al., 1991). In the interpretation below, we consider possible
627 controls on FBOM-$\delta^{13}C$ as needed to explain the observations, but we recognize that other
628 controls may also be important for the data.

There is a clear minimum in ε_{FBOM} just south of the equator, coincident with the local maximum in $[CO_{2(aq)}]$(Fig. 5A/D, 6). This yields the main significant finding of the current study: that planktonic foraminifera show a broad statistically significant anticorrelation between ε_{FBOM} and $[CO_{2(aq)}]$. Both the statistical significance of the anticorrelation and its slope are similar to and generally slightly greater than that observed in SPOM across the surface waters of the global ocean (Rau et al., 1989) (with the exception of *P. obliquiloculata*) (Fig. 7, Table 1).

Laboratory studies have shown that ε_P varies as a function of both $[CO_{2(aq)}]$ and growth rate, which exert opposing pressures on intracellular carbon concentration and thus opposing isotopic effects (Laws et al., 1995). Associated with upwelling, such as in the equatorial Pacific, elevated growth rate concomitant with higher nutrient concentrations is expected to cooccur with the higher $[CO_{2(aq)}]$ (Fig. 5A). The competition of these effects has been invoked to explain the similarity between equatorial and subtropical oligotrophic gyre $\delta^{13}C_{SPOM}$ (Cullen et al., 1992; Goericke and Fry, 1994). This is seen in other organic carbon based geochemical proxies, for which modern surface water equatorial transects do not show the minimum in $\delta^{13}C$ expected if only considering $[CO_{2(aq)}]$ (Pagani et al., 2002).

However, it does not appear that growth rate should have a powerful influence on the variation in ε_{FBOM} in this section of the eastern equatorial Pacific. Anticorrelation of ε_{FBOM} with calculated $\mu/[CO_{2(aq)}]$ (Section 2.3) is only slightly stronger than that with $[CO_{2(aq)}]$ alone (Fig. 8A-D, Table 1). This lack of significant effect derives from the fact that the proportional range in calculated growth rate (26% of mean growth rate) is small compared to that in $[CO_{2(aq)}]$ (39% of mean concentration). This corresponds to a difference in $\delta^{13}C$ of ~1‰ in the case of growth rate (0.14 d^{-1} variation at 7‰ d^{-1}) and ~3‰ for $[CO_{2(aq)}]$ (4.9 µM variation at -0.6‰/ µM)(Rau et al.,

651 1997). Factoring the calculated local growth rate into the correlation increased its significance
652 only for the mixed species and *G. dutertrei* (for both these groups $P < .05$ for $[CO_{2(aq)}]$, and $P <$
653 .001 for $\mu/[CO_{2(aq)}]$; Table 1); in contrast, the significance of *O. universa* decreases ($P < .01$ for
654 $[CO_{2(aq)}]$, and $P < .05$ for $\mu/[CO_{2(aq)}]$). In summary, in this particular system and assuming the
655 accuracy of the satellite-derived phytoplankton growth rate estimates, $[CO_{2(aq)}]$ should be the
656 dominant signal.

657 4.4. Interspecies comparison of ε_{FBOM}

658 It is useful to consider two mechanistic bases for distinguishing between species of
659 planktonic foraminifera: spinose versus non-spinose, and symbiotic versus asymbiotic. We
660 expect the spinosity to principally affect the average isotopic value of FBOM-$\delta^{13}C$ through its
661 effect on the trophic level and thus the $\delta^{13}C$ of organic matter on which the foraminifera feeds.
662 Symbiosis may affect not only the average $\delta^{13}C$ of the organic C available to the foraminiferal
663 host but also its sensitivity to $[CO_{2(aq)}]$, through environmental effects on the isotopic
664 fractionation of the endosymbionts' photosynthesis.

665 The symbionts in planktonic foraminifera are typically either dinoflagellates
666 (Pyrrophyceae) or chrysophytes (Chrysophyceae). The foraminiferal symbiosis with
667 dinoflagellates appears to be both stronger and more integral than the symbiosis with
668 chrysophytes (Hallock, 1999), as supported by i) greater rates of photosynthesis in the former
669 (Rink et al., 1998) and ii) the periodic expulsion of chrysophytes in the latter (Gastrich and
670 Bartha, 1988). Accordingly, below, we mainly distinguish dinoflagellate-bearing foraminifera
671 from both chrysophyte-bearing and asymbiotic foraminifera.

672 Here, we restate our major species-level findings accordingly. First, the differences in
673 mean ε_{FBOM} among species are marginal and do not appear to break down along the above
674 groupings, with the greatest difference occurring between the two chrysophyte-bearing, non-
675 spinose species (*G. menardii* and *P. obliquiloculata*) (Table 1). Second, the dinoflagellate-
676 bearing, spinose species tend to have marginally broader ε_{FBOM} ranges, with both higher (less
677 negative) and lower (more negative) values; however, they are still similar to non-spinose,
678 chrysophyte-bearing *G. menardii* (Table 1). Third, none of the picked foraminifera species have
679 FBOM-$\delta^{13}C$ and ε_{FBOM} values as negative on average as those of the mixed species assemblage,
680 and all appear to vary more (and, excepting *P. obliquiloculata*, covary more strongly with
681 $[CO_{2(aq)}]$) across the study region than the mixed species assemblage (Table 1).

682 Next, we consider each of the three observations listed above. First, what accounts for the
683 similar mean ε_{FBOM} values among species? Second, the data may point to modest but real inter-
684 specific variations in the strength and significance of the anticorrelation with $[CO_{2(aq)}]$, with the
685 possibility of a stronger anticorrelation in the case of dinoflagellate-bearing species; what
686 processes might drive such a difference? Third, to what can we attribute the more positive ε_{FBOM}
687 of the picked species relative to that of the mixed species fraction at certain sites?

688 4.4.1. ε_{FBOM} differences among the studied foraminifera species

689 Foraminifera show a broad dietary range, with some species displaying preferences for
690 high trophic level, some focusing on lower trophic levels, and others dominantly scavenging
691 decomposing material (Schiebel and Hemleben, 2017). Some species are observed to alternate
692 among these behaviors as they progress through their life cycle (Hemleben et al., 2012).

693 Diet is often described as the principal difference in behavior between spinose and non-
694 spinose forms (Hemleben et al., 1985). Laboratory studies suggest that adult spinose
695 foraminifera (including the species *G. sacculifer* and *O. universa* that we measured) feed mostly
696 on zooplankton while non-spinose foraminifera feed primarily on eukaryotic phytoplankton
697 (Anderson et al., 1979; Spindler et al., 1984). Estimates for the trophic offset in $\delta^{13}C$ vary, but
698 common expectations are of a $\delta^{13}C$ increase of roughly 0.4‰ per trophic level (Zanden and
699 Rasmussen, 2001; McCutchan et al., 2003). Given the low amplitude of this offset relative to the
700 variation in measured ε_{FBOM} in this study, it would not be expected to yield a clear, measurable
701 spinose/non-spinose ε_{FBOM} difference. This is especially the case if the largest component of a
702 spinose species diet are zooplankton such as copepods and protozoa, which have a low trophic
703 level (Hobson and Welch, 1992; Gutiérrez-Rodríguez et al., 2014).

704 Moreover, the available laboratory and field data on foraminiferal food preferences may
705 not reflect actual feeding patterns, given the potential for variation in food scarcity and other
706 ecosystem pressures as well as other considerations. Specifically, diets may be more similar
707 between spinose and non-spinose species than has been suggested by laboratory studies. Non-
708 spinose species tend to settle at the bottom of culture vessels. This prevents them from extending
709 their rhizopodial nets and thus impairs their feeding efficiency (Schiebel and Hemleben, 2017).
710 In addition, trophic effects may be complicated by certain components of prey that may not be
711 digestible (such as chitinous carapaces) (Horst, 1989) or active selection of particular tissues,
712 which can have distinct isotopic signatures (Macko et al., 1990) (Fig. 1, right side).

713 The similarity of FBOM-$\delta^{13}C$ between spinose and non-spinose species (and across all
714 species investigated here) has a broad range of possible causes and explanations. Among the
715 different species measured, two are shallow dwellers (*O. universa* with an average inferred depth

716 of 50 m and *G. sacculifer*, 30 m), and 3 are deeper dwelling *G. menardii* (50-75 m) and *P.*
717 *obliquiloculata* (65-110 m), and *G. dutertrei* (75-135 m)) (Emiliani, 1971; Faul et al., 2000;
718 Farmer et al., 2007). The shallower dwelling species are more likely to be active feeders, while
719 the deeper dwellers are more likely to be detritus feeders (Rau et al., 1992; Nakatsuka et al.,
720 1997). However, depth gradients in $\delta^{13}C_{SPOM}$ and the $\delta^{13}C$ relationship between suspended and
721 sinking POM are both poorly known, and the potential for vertical migration may blur any such
722 depth effect.

723 Most foraminifera appear to have algal symbionts. The impact of symbiont-derived
724 photosynthates might be illuminated by comparing the bulk biomass of the $\delta^{13}C$ of symbiotic and
725 asymbiotic foraminifera, and perhaps by comparison to an analogous 'holobiont' system such as
726 corals. In the culture experiment of Uhle et al. (1997) described above, a biomass $\delta^{13}C$ difference
727 between *O. universa* and *G. bulloides* was attributed to the contribution of photosynthetic carbon
728 from the symbionts in *O. universa*, which would require that the $\delta^{13}C$ of carbon sourced from the
729 dinoflagellates is higher than the diet (which was -15‰ in that experiment). This is supported by
730 $\delta^{13}C$ measurements of symbiotic dinoflagellates in corals: -10‰ in *Heliofungia actiniformis* , -
731 13‰ in *Pocillopora damicornis* (Hoegh-Guldberg et al., 2004) and -12.2‰ in *Montastraea*
732 *faveolata* (Swart et al., 2005).

733 Although foraminifera are small enough for molecular diffusion to be relatively rapid
734 (Jørgensen et al., 1985), laboratory studies indicate that there are steep gradients in both O_2 and
735 pH extending up to 1 mm from the shell surface. In direct light, the pH in the "symbiont cloud"
736 of *O. universa* can reach 8.7-8.8, which is attributed to the drawdown of CO_2 by the
737 photosynthetic activity of the symbionts. In the dark, the pH in the symbiont cloud drops to 7.9,
738 which is attributed to the release of CO_2 by foraminiferal respiration. The elevated pH in the

739 symbiont cloud under well-lit conditions suggests that, while photosynthesis is occurring when
740 the symbionts are outside the host, exchange with the broader environment is reduced by a
741 diffusive boundary layer (DBL). This would indicate that CO_2 levels within the symbiont cloud
742 are often very low, which should decrease ε_p and weaken the anticorrelation between
743 environmental [$CO_{2(aq)}$] and foraminiferal biomass $\delta^{13}C$.

744 Despite the existence of conditions conducive to high-$\delta^{13}C$ photosynthates, the $\delta^{13}C$
745 difference observed between the symbiotic and asymbiotic species by Uhle et al. (1997) was
746 small (~1.1‰), and there is no discernable offset in our core top measurements of ε_{FBOM}. This
747 leads us to consider critically the two assumptions that underlie the expectation of a higher
748 ε_{FBOM} in symbiotic foraminifera. The first is that, in order to be observable, carbon sourced from
749 endosymbionts must contribute a significant proportion of the organic carbon to the host. The
750 second is that this contribution is consistently higher in $\delta^{13}C$ than the diet.

751 The evidence for the first of these assumptions seems strong. Laboratory experiments
752 suggest that a substantial fraction of the host's carbon budget derives from symbiont
753 photosynthesis. For example, in radiocarbon incubation studies, the respiration rate of the whole
754 'holobiont' is on average only 50(±6)% of the rate of gross photosynthesis by the symbionts
755 (Köhler-Rink and Kühl, 2000a). While laboratory experiments may not necessarily represent in
756 situ conditions accurately, there are some field observations to support these studies. At the most
757 basic level, the extreme prevalence of the comparatively small number of symbiont-bearing
758 species argues for a clear benefit to harboring symbionts. Population surveys suggest that >90%
759 of surface dwelling foraminifera are symbiotic (Almogi-Labin, 1984) and produce ~20% of the
760 calcium carbonate fixed in the world's ocean each year, despite representing less than 10% of
761 extant foraminifera families (Lee and Hallock, 1987). There is also isotopic evidence for the

762 significance of symbiont activity, as seen in the consistent differences in the calcium carbonate
763 $\delta^{13}C$ between symbiotic and asymbiotic foraminiferal tests (Sautter and Thunell, 1991), where
764 the preferential fixation of $^{12}CO_{2(aq)}$ leads to residual ^{13}C enrichment and higher carbonate $\delta^{13}C$.
765 Measurements show that symbiont densities and photosynthetic activity scale with foraminifera
766 size and light intensity, with increases in each corresponding to higher carbonate $\delta^{13}C$ (Rink et
767 al., 1998).

768 Thus, in order to explain the lack of $\delta^{13}C$ difference between symbiotic and asymbiotic
769 foraminifera, it would appear that we must turn to the $\delta^{13}C$ of the symbionts. The most obvious
770 hypothesis is that the distinction in carbon availability between the symbiont cloud and ambient
771 water is weaker than observed in the lab. There is some support for this possibility. Lower levels
772 of photosynthetic activity are observed to reduce the gradient between the immediate exterior of
773 the foraminifer and the surrounding water (Jørgensen et al., 1985). As the photosynthetic activity
774 of the algal symbiont community fluctuates as a function of degree of light saturation (Jørgensen
775 et al., 1985), the symbiont clouds of foraminifera in the open ocean may not achieve the high
776 productivity of the laboratory experiments in which the elevated pH of the symbiont cloud has
777 been documented. Symbiont photosynthetic rate varies with light level (Jørgensen et al., 1985;
778 Rink et al., 1998). Under irradiance levels consistent with ~50 m depth under sunny conditions in
779 San Pedro Basin near Catalina Island (100 µmol photons m^{-2} s^{-1}), pH at the edge of the symbiont
780 cloud can approach (come within 0.1 of) ambient sea water values (Rink et al., 1998). If so, this
781 would decrease both the $\delta^{13}C$ of symbiont-derived carbon, which would reduce the overall
782 impact on ε_{FBOM}.

783 Additionally, small scale turbulence in the ocean may reduce the chemical gradients
784 associated with the symbiont cloud relative to that observed in the laboratory. Experiments that

varied flow rate saw a corresponding decrease in DBL thickness from 400-700 μm in stagnant conditions to 100-175 μm with flow (Köhler-Rink and Kühl, 2000a). Thinner DBL yields higher concentration gradients and thus higher solvent flux (Patterson et al., 1991), thus reducing the potential for inorganic carbon limitation. Indeed, at higher flow rates, both gross photosynthesis and dark respiration showed a significant increase (Köhler-Rink and Kühl, 2000b).

An internal pool of low-$\delta^{13}C$ metabolic inorganic carbon has been demonstrated in perforate foraminifera (ten Kuile and Erez, 1987) (Fig. 1, right side). Foraminifera can grow to prodigious size relative to other protists. As size increases, so does the quantity of metabolites that must be removed, a problem that may be alleviated by the consumption of these metabolites by the symbionts (Hallock, 1999). Exchange between the interior and exterior of the shell through the pores in the test of perforate foraminifera is observed (ten Kuile and Erez, 1987). The net effect of the supply of low-$\delta^{13}C$ respiratory CO_2 from within the shell to the photosynthesizing symbionts in the symbiont cloud is uncertain, but it presumably pushes the symbionts toward the $\delta^{13}C$ of the host's diet (Fig. 1, right side). Micro-electrode measurements of O_2 indicate significant inorganic carbon fluxes (Jørgensen et al., 1985), which implies that the low-$\delta^{13}C$ CO_2 from the host may work against the tendency for a high $\delta^{13}C$ in the phytosymbionts, tending to decrease the $\delta^{13}C$ difference between foraminifera with and without dinoflagellates.

Finally, the calcification of the foraminiferal host and its effect on the inorganic carbon pool from which the test precipitates must be considered. Calcification works to lower pH and convert HCO_3^- to CO_2. Under most conditions, the calcification-driven rise in aqueous CO_2 concentration would tend to lower the $\delta^{13}C$ of the photosynthate produced by the symbionts (McConnaughey, 1989; Romanek et al., 1992), making it more similar to the $\delta^{13}C$ of open water

808 phytoplankton photosynthate. Thus, a higher calcification rate in symbiont-bearing foraminifera
809 would make the FBOM-$\delta^{13}C$ of symbiont-bearing foraminifera more similar to that of
810 asymbiotic species than would otherwise be the case. We recognize that this proposal has a range
811 of weaknesses. In particular, the rate of calcification may not be comparable to symbiont
812 photosynthesis (Wolf-Gladrow et al., 1999; Zeebe, 1999), and this calcification is spatially
813 removed from the symbiont cloud.

814 #### 4.4.2. Interpretation of species-specific covariation of ε_{FBOM} with $[CO_{2(aq)}]$

815 The data suggest that an equivalent or higher degree of anticorrelation between $[CO_{2(aq)}]$ and
816 ε_{FBOM} is achieved in symbiotic foraminifera, contrary to expectations. We raise three possible
817 explanations for this unexpected finding, with the important qualification that we are not
818 confident that the finding will persist as additional studies are conducted.

819 First, the $\delta^{13}C$ of directly symbiont-derived organic carbon would lack the isotopic
820 variability associated with the taxonomy of the photosynthesizer or with the trophic,
821 decompositional, and/or metabolic processes associated with the foraminifer acquiring and
822 digesting the organic carbon from the water column.

823 Second, lower $[CO_{2(aq)}]$ in the symbiont cloud may strengthen the dependence of
824 photosynthate $\delta^{13}C$ on $[CO_{2(aq)}]$. This possibility may involve the contribution of HCO_3^- to
825 symbiont carbon fixation (Fig. 1, left side). Symbiont photosynthesis may become carbon-limited
826 in response to low $[CO_{2(aq)}]$. This is made more likely by dinoflagellates being both relatively
827 large and having high carbon demands and thus being more likely to be heavily constrained by a
828 diffusion-only supply of inorganic carbon, which may elicit the use of HCO_3^- (Miller et al., 1990;
829 Burkhardt et al., 2001). Although the system is complex, the expected effect of HCO_3^- use is to

reduce isotopic fractionation associated with fixation. Thus, if the dinoflagellates rely on HCO_3^- at low ambient $[CO_{2(aq)}]$, then the $\delta^{13}C$ of the organic C fixed by the symbionts may show a stronger anticorrelation with $[CO_{2(aq)}]$ than without this process. This would amplify the degree to which the ε_{FBOM} of symbiont-bearing foraminifera covaries with $[CO_{2(aq)}]$. That is, it may explain the slight elevation in FBOM-$\delta^{13}C$ in dinoflagellate-bearing forms from the locations with the lowest $[CO_{2(aq)}]$, while not applying to the higher-$[CO_{2(aq)}]$ locations where active carbon uptake may not be required.

Third, the growth environment of endosymbionts may be more uniform than that experienced by free-living phytoplankton across the equatorial Pacific. The principal influences on ε_p are commonly held to be growth rate (μ) and $[CO_{2(aq)}]$, which have opposite effects (eqn. 5), and both are elevated in the upwelling zone of the equatorial Pacific. In the equatorial Pacific, spatial variation in phytoplankton productivity is largely controlled by nutrient availability. Thus, FBOM-$\delta^{13}C$ and $[CO_{2(aq)}]$ might be better correlated in symbiont-bearing foraminifera than in symbiont-barren species if their dinoflagellate symbionts experience a weaker gradient in nutrient limitation than that experienced by free-living phytoplankton that are the origin of SPOM in surface waters and ultimately the external food to foraminifera. Foraminiferal symbionts are observed to consume the NH_4^+ and PO_4^{3-} that is produced as metabolic waste by the foraminiferal host (ter Kuile et al., 1989). While NO_3^- and PO_4^{3-} may be taken up from the environment, symbionts must derive a considerable portion of their nutrient sources from their hosts, as evidenced by the finding that a single large adult *O. universa* is 20,000 times more productive than the equivalent volume of seawater (Spero and Parker, 1985). This suggests that, for a given change in the nutrient concentrations in surface waters, the productivity of free-living phytoplankton would be altered more than that of foraminifera-associated dinoflagellates. This

productivity response would tend to result in a stronger anticorrelation between ε_{FBOM} and $[CO_{2(aq)}]$ for the symbiotic foraminifera relative to facultatively symbiotic or asymbiotic forms.

4.4.3. Isotopic offsets between mixed and picked species

The mean value of the ε_{FBOM} of the mixed species most closely matches the ε_{FBOM} of the lowest-$\delta^{13}C$ picked species (*G. menardii*), despite it being an aggregate of each of the individually picked species. These differences are slight and may be affected by the preponderance of *G. menardii*, which was apparent in visual inspections of the coarse fraction). Mixed species $\delta^{18}O$ also suggests that this component is dominated by a deeper dwelling species.

There are three sample sites where the mixed species size fraction is more negative than each of the picked species. If mixed species mean ε_{FBOM} at these three sites is replaced with the composite mean of the individually picked species, then the mixed species average across all sites is within 0.09‰ of that of *G. menardii*. The low ε_{FBOM} of the mixed species assemblage at these sites suggests the presence of an otherwise-unsampled foraminifera or another organic C-containing component. Visual inspection of the mixed species samples indicates only trace quantities of sponge spicules, dinoflagellate cysts and radiolaria. Nevertheless, the relative contribution of one of these contaminants might be disproportionately enhanced by the cleaning process, which is quite destructive to carbonate but less so to some of the other material. Reanalysis of these samples after more careful inspection and the removal non-foraminiferal material brought the anomalous points to within 0.2‰ of picked species (data not shown). However, the mixed species $\delta^{13}C$ still remained on average low, roughly equivalent to the most negative individually picked species.

5. **Conclusions**

This study represents our first effort to measure FBOM-$\delta^{13}C$ and deconvolve the factors controlling it. Our results indicate that FBOM-$\delta^{13}C$ may be suitable as a proxy for the reconstruction of $[CO_{2(aq)}]$ over the range that occurs in the modern ocean. Contrary to expectations, we observe broad a similarity in FBOM-$\delta^{13}C$ across all measured species. Moreover, against our initial expectations, the FBOM-$\delta^{13}C$ of species with more obligate symbiont associations covaried slightly more strongly with $[CO_{2(aq)}]$ than did that of species with weaker symbiotic relationships. These findings raise the surprising possibility that the photosynthate $\delta^{13}C$ of the dinoflagellate endosymbionts in planktonic foraminifera is uniquely suited to track $[CO_{2(aq)}]$. These results call for further study, with additional species and across different environmental conditions. They also call for further investigation into the internal carbon cycling of planktonic foraminifera. Nevertheless, the existence of the relationship across all picked species and within the mixed species fraction bodes well for the utility of planktonic foraminifera FBOM-$\delta^{13}C$ in reconstructing past changes in $[CO_{2(aq)}]$.

889 **Acknowledgements**

890 This research used samples provided by the RSMAS core repository (with special thanks to Dr.
891 Larry C. Peterson). The World Climate Research Program's Working Group on Coupled
892 Modeling, which is responsible for CMIP, is acknowledged for their publicly available model
893 output. Funding: This work was supported by the Dean for Research Innovation Fund of
894 Princeton University and US NSF grant OCE-1060947 (D.M.S), and by the Max Planck Society
895 (G.H.H.). Author Contributions: D.M.S. conceptualized the study, in consultation with A.M.G
896 and G.H.H.; S.O., K.A.S., and D.M.S. designed and built instrumentation, with input from
897 A.M.G.; K.A.S. developed methodology; K.A.S carried out the carbon and oxygen isotopic
898 measurements; K.A.S. and D.M.S. performed data analysis. K.A.S. and D.M.S prepared the first
899 draft of the manuscript. All authors contributed to the preparation of the final manuscript.
900 Competing interests: The authors have no competing interests to declare.

901

902 Citations

903 Abelson P. H. and Hoering T. C. (1961) Carbon Isotope Fractionation in Formation of Amino Acids by
904 Photosynthetic Organisms. *Proc. Natl. Acad. Sci. U. S. A.* **47**, 623–632.

905 Allan W. H. Bé, Hemleben C., Anderson O. R. and Spindler M. (1979) Chamber Formation in Planktonic
906 Foraminifera. *Micropaleontology* **25**, 294–307.

907 Allan W. H. Bé, Hemleben C., Anderson O. R., Spindler M., Hacunda J. and Tuntivate-Choy S. (1977)
908 Laboratory and Field Observations of Living Planktonic Foraminifera. *Micropaleontology* **23**,
909 155–179.

910 Almogi-Labin A. (1984) Population dynamics of planktic Foraminifera and Pteropoda Gulf of Aqaba, Red
911 Sea. In Proceedings of the Koninklke Nederlandse Akademie van Wetenschappen. Series B.
912 Palaeontology, geology, physics and chemistry. North-Holland. pp. 481–511.

913 Anderson O. R., Spindler M., Bé A. W. H. and Hemleben Ch. (1979) Trophic activity of planktonic
914 foraminifera. *J. Mar. Biol. Assoc. U. K.* **59**, 791.

915 Bakker D. C. E., Pfeil B., Landa C. S., Metzl N., O'Brien K. M., Olsen A., Smith K., Cosca C., Harasawa S.,
916 Jones S. D., Nakaoka S.-I., Nojiri Y., Schuster U., Steinhoff T., Sweeney C., Takahashi T., Tilbrook
917 B., Wada C., Wanninkhof R., Alin S. R., Balestrini C. F., Barbero L., Bates N. R., Bianchi A. A.,
918 Bonou F., Boutin J., Bozec Y., Burger E. F., Cai W.-J., Castle R. D., Chen L., Chierici M., Currie K.,
919 Evans W., Featherstone C., Feely R. A., Fransson A., Goyet C., Greenwood N., Gregor L., Hankin
920 S., Hardman-Mountford N. J., Harlay J., Hauck J., Hoppema M., Humphreys M. P., Hunt C. W.,
921 Huss B., Ibánhez J. S. P., Johannessen T., Keeling R., Kitidis V., Körtzinger A., Kozyr A.,
922 Krasakopoulou E., Kuwata A., Landschützer P., Lauvset S. K., Lefèvre N., Lo Monaco C., Man ke A.,
923 Mathis J. T., Merlivat L., Millero F. J., Monteiro P. M. S., Munro D. R., Murata A., Newberger T.,
924 Omar A. M., Ono T., Paterson K., Pearce D., Pierrot D., Robbins L. L., Saito S., Salisbury J.,
925 Schlitzer R., Schneider B., Schweitzer R., Sieger R., Skjelvan I., Sullivan K. F., Sutherland S. C.,
926 Sutton A. J., Tadokoro K., Telszewski M., Tuma M., van Heuven S. M. A. C., Vandemark D., Ward
927 B., Watson A. J. and Xu S. (2016) A multi-decade record of high-quality $f$$CO_2$ data in version 3
928 of the Surface Ocean CO_2 Atlas (SOCAT). *Earth Syst. Sci. Data* **8**, 383–413.

929 Barnes C., Sweeting C., Jennings S., Barry J. and Polunin N. (2007) *Effect of temperature and ration size*
930 *on carbon and nitrogen stable isotope trophic fractionation*.,

931 Bates T. S., Kelly K. C. and Johnson J. E. (1993) Concentrations and fluxes of dissolved biogenic gases
932 (DMS, CH4, CO, CO2) in the equatorial Pacific during the SAGA 3 experiment. *J. Geophys. Res.*
933 *Atmospheres* **98**, 16969–16977.

934 Beerling D. J. and Royer D. L. (2011) Convergent Cenozoic CO2 history. *Nat. Geosci.* **4**, 418–420.

935 Behrenfeld M. J., Boss E., Siegel D. A. and Shea D. M. (2005) Carbon-based ocean productivity and
936 phytoplankton physiology from space. *Glob. Biogeochem. Cycles* **19**. Available at:
937 https://doi.org/10.1029/2004GB002299 [Accessed November 28, 2018].

938 Bemis B. E., Spero H. J., Bijma J. and Lea D. W. (1998) Reevaluation of the oxygen isotopic composition of
939 planktonic foraminifera: Experimental results and revised paleotemperature equations.
940 *Paleoceanography* **13**, 150–160.

941 Benner R., Biddanda B., Black B. and McCarthy M. (1997) Abundance, size distribution, and stable
942 carbon and nitrogen isotopic compositions of marine organic matter isolated by tangential-flow
943 ultrafiltration. *Mar. Chem.* **57**, 243–263.

944 Bidigare R. R., Kennicutt M. C., Keeney-Kennicutt W. L. and Macko S. A. (1991) Isolation and purification
945 of chlorophylls a and b for the determination of stable carbon and nitrogen isotope
946 compositions. *Anal. Chem.* **63**, 130–133.

947 Brassell S. C. (2014) Climatic influences on the Paleogene evolution of alkenones. *Paleoceanography* **29**,
948 255–272.

949 Brassell S., Eglinton G., Marlowe I., Pflaumann U. and Sarnthein M. (1986) Molecular stratigraphy: a new
950 tool for climatic assessment. *Nature* **320**, 129.

951 Burkhardt S., Amoroso G., Riebesell U. and Sültemeyer D. (2001) CO2 and HCO3 ⇵ uptake in marine
952 diatoms acclimated to different CO2 concentrations. *Limnol. Oceanogr.* **46**, 1378–1391.

953 Burkhardt S., Riebesell U. and Zondervan I. (1999) Effects of growth rate, CO2 concentration, and cell
954 size on the stable carbon isotope fractionation in marine phytoplankton. *Geochim. Cosmochim.*
955 *Acta* **63**, 3729–3741.

956 Cassar N., Laws E. A., Bidigare R. R. and Popp B. N. (2004) Bicarbonate uptake by Southern Ocean
957 phytoplankton. *Glob. Biogeochem. Cycles* **18**.

958 Chen M., Guo L., Ma Q., Qiu Y., Zhang R., Lv E. and Huang Y. (2006) Zonal patterns of δ13C, δ15N and
959 210Po in the tropical and subtropical North Pacific. *Geophys. Res. Lett.* **33**. Available at:
960 https://agupubs.onlinelibrary.wiley.com/doi/abs/10.1029/2005GL025186 [Accessed January 29,
961 2019].

962 Craig H. (1957) Isotopic standards for carbon and oxygen and correction factors for mass-spectrometric
963 analysis of carbon dioxide. *Geochim. Cosmochim. Acta* **12**, 133–149.

964 Cullen J. J., Lewis M. R., Davis C. O. and Barber R. T. (1992) Photosynthetic characteristics and estimated
965 growth rates indicate grazing is the proximate control of primary production in the equatorial
966 Pacific. *J. Geophys. Res.* **97**, 639.

967 Degens E. T., Behrendt M., Gotthardt B. and Reppmann E. (1968) Metabolic fractionation of carbon
968 isotopes in marine plankton—II. Data on samples collected off the coasts of Peru and Ecuador.
969 *Deep Sea Res. Oceanogr. Abstr.* **15**, 11–20.

970 DeNiro M. J. and Epstein S. (1977) Mechanism of carbon isotope fractionation associated with lipid
971 synthesis. *Science* **197**, 261–263.

972 Druffel E. R. M., Williams P. M., Bauer J. E. and Ertel J. R. (1992) Cycling of dissolved and particulate
973 organic matter in the open ocean. *J. Geophys. Res. Oceans* **97**, 15639–15659.

974 Eadie B. J. and Jeffrey L. M. (1973) δ13C analyses of oceanic particulate organic matter. *Mar. Chem.* **1**,
975 199–209.

976 Emiliani C. (1971) Depth habitats of growth stages of pelagic foraminifera. *Science* **173**, 1122–1124.

977 Eppley R. W. (1972) Temperature and phytoplankton growth in the sea. *Fish Bull* **70**, 1063–1085.

978 Erez J. and Luz B. (1983) Experimental paleotemperature equation for planktonic foraminifera. *Geochim.*
979 *Cosmochim. Acta* **47**, 1025–1031.

980 Fairbanks R. G., Sverdlove M., Free R., Wiebe P. H. and Bé A. W. H. (1982) Vertical distribution and
981 isotopic fractionation of living planktonic foraminifera from the Panama Basin. *Nature* **298**, 841–
982 844.

983 Farmer E. C., Kaplan A., de Menocal P. B. and Lynch-Stieglitz J. (2007) Corroborating ecological depth
984 preferences of planktonic foraminifera in the tropical Atlantic with the stable oxygen isotope
985 ratios of core top specimens: FORAM DEPTH PREFERENCES. *Paleoceanography* **22**, n/a-n/a.

986 Farquhar G. D., Ehleringer J. R. and Hubick K. T. (1989) Carbon isotope discrimination and
987 photosynthesis. *Annu. Rev. Plant Biol.* **40**, 503–537.

988 Farquhar G. D., O'Leary M. H. and Berry J. A. (1982) c. *Funct. Plant Biol.* **9**, 121–137.

989 Faul K. L., Ravelo A. C. and Delaney M. L. (2000) RECONSTRUCTIONS OF UPWELLING, PRODUCTIVITY,
990 AND PHOTIC ZONE DEPTH IN THE EASTERN EQUATORIAL PACIFIC OCEAN USING PLANKTONIC
991 FORAMINIFERAL STABLE ISOTOPES AND ABUNDANCES. *J. Foraminifer. Res.* **30**, 110–125.

992 Fhlaithearta S. N., Ernst S. R., Nierop K. G., de Lange G. J. and Reichart G.-J. (2013) Molecular and
993 isotopic composition of foraminiferal organic linings. *Mar. Micropaleontol.* **102**, 69–78.

994 Fitt W., K. McFarland F., Warner M. and C. Chilcoat G. (2000) *Seasonal Patterns of Tissue Biomass and*
995 *Densities of Symbiotic Dinoflagellates in Reef Corals and Relation to Coral Bleaching* .,

996 Ford H. L., McChesney C. L., Hertzberg J. E. and McManus J. F. (2018) A Deep Eastern Equatorial Pacific
997 Thermocline During the Last Glacial Maximum. *Geophys. Res. Lett.* **45**, 11,806-11,816.

998 Foster G. (2008) Seawater pH, pCO2 and [CO2− 3] variations in the Caribbean Sea over the last 130 kyr:
999 A boron isotope and B/Ca study of planktic foraminifera. *Earth Planet. Sci. Lett.* **271**, 254–266.

1000 Francois R., Altabet M. A., Goericke R., McCorkle D. C., Brunet C. and Poisson A. (1993) Changes in the
1001 δ13C of surface water particulate organic matter across the subtropical convergence in the SW
1002 Indian Ocean. *Glob. Biogeochem. Cycles* **7**, 627–644.

1003 Freudenthal T., Wagner T., Wenzhöfer F., Zabel M. and Wefer G. (2001) Early diagenesis of organic
1004 matter from sediments of the eastern subtropical Atlantic: evidence from stable nitrogen and
1005 carbon isotopes. *Geochim. Cosmochim. Acta* **65**, 1795–1808.

1006 Frouin R., Lingner D. W., Gautier C., Baker K. S. and Smith R. C. (1989) A simple analytical formula to
1007 compute clear sky total and photosynthetically available solar irradiance at the ocean surface. *J.*
1008 *Geophys. Res. Oceans* **94**, 9731–9742.

1009 Galimov E. (2012) *The biological fractionation of isotopes*., Elsevier.

1010 Gastrich M. and Bartha R. (1988) Primary productivity in the planktonic foraminifer Globigerinoides
1011 ruber (d'Orbigny). *J. Foraminifer. Res.* **18**, 137–142.

1012 Geider R. and La Roche J. (2002) Redfield revisited: variability of C:N:P in marine microalgae and its
1013 biochemical basis. *Eur. J. Phycol.* **37**, 1–17.

1014 Goericke R. and Fry B. (1994) Variations of marine plankton δ13C with latitude, temperature, and
1015 dissolved CO2 in the world ocean. *Glob. Biogeochem. Cycles* **8**, 85–90.

1016 Goericke R., Montoya J. and Fry B. (1994) *Physiology of isotope fractionation in algae and*
1017 *cyanobacteria*.,

1018 Goreau T. (1977) Coral skeletal chemistry: physiological and environmental regulation of stable isotopes
1019 and trace metals in Montastrea annularis. *Proc. R. Soc. Lond. B Biol. Sci.* **196**, 291–315.

1020 Greenop R., Foster G. L., Wilson P. A. and Lear C. H. (2014) Middle Miocene climate instability associated
1021 with high-amplitude CO2 variability. *Paleoceanography* **29**, 845–853.

1022 Gutiérrez-Rodríguez A., Décima M., Popp B. N. and Landry M. R. (2014) Isotopic invisibility of protozoan
1023 trophic steps in marine food webs. *Limnol. Oceanogr.* **59**, 1590–1598.

1024 Hallock P. (1999) Symbiont-bearing Foraminifera. In *Modern Foraminifera* Springer Netherlands,
1025 Dordrecht. pp. 123–139. Available at: http://link.springer.com/10.1007/0-306-48104-9_8
1026 [Accessed February 18, 2019].

1027 Hatch J. R. and Leventhal J. S. (1997) Early diagenetic partial oxidation of organic matter and sulfides in
1028 the Middle Pennsylvanian (Desmoinesian) Excello Shale member of the Fort Scott Limestone and
1029 equivalents, northern Midcontinent region, USA. *Chem. Geol.* **134**, 215–235.

1030 Hayes J. M. (1993) Factors controlling 13C contents of sedimentary organic compounds: Principles and
1031 evidence. *Mar. Sediments Burial Pore Water Chem. Microbiol. Diagenesis* **113**, 111–125.

1032 Hayes J. M. (2001) Fractionation of carbon and hydrogen isotopes in biosynthetic processes. *Rev.*
1033 *Mineral. Geochem.* **43**, 225–277.

1034 Hemleben C., Spindler M. and Anderson O. R. (2012) *Modern planktonic foraminifera*., Springer Science
1035 & Business Media.

1036 Hemleben C., Spindler M., Breitinger I. and Deuser W. G. (1985) Field and laboratory studies on the
1037 ontogeny and ecology of some globorotaliid species from the Sargasso Sea off Bermuda. *J.*
1038 *Foraminifer. Res.* **15**, 254–272.

1039 Higgins J. A., Kurbatov A. V., Spaulding N. E., Brook E., Introne D. S., Chimiak L. M., Yan Y., Mayewski P. A.
1040 and Bender M. L. (2015) Atmospheric composition 1 million years ago from blue ice in the Allan
1041 Hills, Antarctica. *Proc. Natl. Acad. Sci.* **112**, 6887–6891.

1042 Hinga K. R., Arthur M. A., Pilson M. E. and Whitaker D. (1994) Carbon isotope fractionation by marine
1043 phytoplankton in culture: the effects of CO2 concentration, pH, temperature, and species. *Glob.*
1044 *Biogeochem. Cycles* **8**, 91–102.

1045 Hobson K. and Welch H. (1992) Determination of trophic relationships within a high Arctic marine food
1046 web using δ13C and δ15N analysis. *Mar. Ecol. Prog. Ser.* **84**, 9–18.

1047 Hoegh-Guldberg O., Muscatine L., Goiran C., Siggaard D. and Marion G. (2004) Nutrient-induced
1048 perturbations to δ13C and δ15N in symbiotic dinoflagellates and their coral hosts. *Mar. Ecol.*
1049 *Prog. Ser.* **280**, 105–114.

1050 Hönisch B. and Hemming N. G. (2004) Ground-truthing the boron isotope-paleo-pH proxy in planktonic
1051 foraminifera shells: Partial dissolution and shell size effects: GROUND-TRUTHING THE δ^{11} B-
1052 PALEO-PH PROXY. *Paleoceanography* **19**, n/a-n/a.

1053 Hopkinson B. M., Dupont C. L., Allen A. E. and Morel F. M. M. (2011) Efficiency of the CO_2-concentrating
1054 mechanism of diatoms. *Proc. Natl. Acad. Sci.* **108**, 3830.

1055 Horst M. N. (1989) Molecular and cellular aspects of chitin synthesis in larval Artemia. In *Cell and*
1056 *Molecular Biology of Artemia Development* Springer. pp. 59–76.

1057 Hu C., Lee Z. and Franz B. (2012) Chlorophyll aalgorithms for oligotrophic oceans: A novel approach
1058 based on three-band reflectance difference. *J. Geophys. Res. Oceans* **117**.

1059 Hwang J., Druffel E. R. M., Griffin S., Smith K. L., Baldwin R. J. and Bauer J. E. (2004) Temporal variability
1060 of Δ^{14}C, δ^{13}C, and C/N in sinking particulate organic matter at a deep time series station in the
1061 northeast Pacific Ocean: TEMPORAL VARIABILITY OF SINKING POM. *Glob. Biogeochem. Cycles*
1062 **18**, n/a-n/a.

1063 Ingalls A. E., Lee C. and Druffel E. R. M. (2003) Preservation of organic matter in mound-forming coral
1064 skeletons. *Geochim. Cosmochim. Acta* **67**, 2827–2841.

1065 Jasper J., Hayes J., Mix A. and G Prahl F. (1994) *Photosynthetic fractionation of 13C and concentrations of*
1066 *dissolved CO2 in the central equatorial Pacific during the last 255 000 yreas*.,

1067 Jasper J. P. and Gagosian R. B. (1989) Glacial–interglacial climatically forced δ13C variations in
1068 sedimentary organic matter. *Nature* **342**, 60.

1069 Jasper J. P. and Hayes J. M. (1990) A carbon isotope record of CO2 levels during the late Quaternary.
1070 *Nature* **347**, 462.

1071 Jørgensen B. B., Erez J., Revsbech P. and Cohen Y. (1985) Symbiotic photosynthesis in a planktonic
1072 foraminiferan, Globigerinoides sacculifer (Brady), studied with microelectrodes1. *Limnol.*
1073 *Oceanogr.* **30**, 1253–1267.

1074 Keller K. and Morel F. (1999) A model of carbon isotopic fractionation and active carbon uptake in
1075 phytoplankton. *Mar. Ecol. Prog. Ser.* **182**, 295–298.

1076 King K. and Hare P. E. (1972) Amino Acid Composition of Planktonic Foraminifera : A Paleobiochemical
1077 Approach to Evolution. *Science* **175**, 1461.

1078 Köhler-Rink S. and Kühl M. (2000a) Microsensor studies of photosynthesis and respiration in larger
1079 symbiotic foraminifera. I The physico-chemical microenvironment of Marginopora vertebralis,
1080 Amphistegina lobifera and Amphisorus hemprichii. *Mar. Biol.* **137**, 473–486.

1081 Köhler-Rink S. and Kühl M. (2000b) Microsensor studies of photosynthesis and respiration in larger
1082 symbiotic foraminifera. I The physico-chemical microenvironment of Marginopora vertebralis,
1083 Amphistegina lobifera and Amphisorus hemprichii. *Mar. Biol.* **137**, 473–486.

1084 Kucera M. (2007) Chapter Six Planktonic Foraminifera as Tracers of Past Oceanic Environments. In
1085 *Developments in Marine Geology* (eds. C. Hillaire–Marcel and A. De Vernal). Elsevier. pp. 213–
1086 262. Available at: http://www.sciencedirect.com/science/article/pii/S1572548007010111.

1087 ten Kuile B. and Erez J. (1987) Uptake of inorganic carbon and internal carbon cycling in symbiont-
1088 bearing benthonic foraminifera. *Mar. Biol.* **94**, 499–509.

1089 ter Kuile B., Erez J. and Padan E. (1989) Mechanisms for the uptake of inorganic carbon by two species of
1090 symbiont-bearing foraminifera. *Mar. Biol.* **103**, 241–251.

1091 Laws E. A. and Bannister T. T. (1980) Nutrient- and light-limited growth of Thalassiosira fluviatilis in
1092 continuous culture, with implications for phytoplankton growth in the ocean1. *Limnol.*
1093 *Oceanogr.* **25**, 457–473.

1094 Laws E. A., Popp B. N., Bidigare R. R., Kennicutt M. C. and Macko S. A. (1995) Dependence of
1095 phytoplankton carbon isotopic composition on growth rate and [CO2)aq: Theoretical
1096 considerations and experimental results. *Geochim. Cosmochim. Acta* **59**, 1131–1138.

1097 Laws E. A., Popp B. N., Cassar N. and Tanimoto J. (2002) 13C discrimination patterns in oceanic
1098 phytoplankton: likely influence of CO2 concentrating mechanisms, and implications for
1099 palaeoreconstructions. *Funct. Plant Biol.* **29**, 323–333.

1100 Lea D. W., Pak D. K. and Spero H. J. (2000) Climate Impact of Late Quaternary Equatorial Pacific Sea
1101 Surface Temperature Variations. *Science* **289**, 1719.

1102 Lee J. J. and Hallock P. (1987) Algal Symbiosis as the Driving Force in the Evolution of Larger Foraminifera
1103 a. *Ann. N. Y. Acad. Sci.* **503**, 330–347.

1104 Lehmann M. F., Bernasconi S. M., Barbieri A. and McKenzie J. A. (2002) Preservation of organic matter
1105 and alteration of its carbon and nitrogen isotope composition during simulated and in situ early
1106 sedimentary diagenesis. *Geochim. Cosmochim. Acta* **66**, 3573–3584.

1107 Lüthi D., Le Floch M., Bereiter B., Blunier T., Barnola J.-M., Siegenthaler U., Raynaud D., Jouzel J., Fischer
1108 H., Kawamura K. and Stocker T. F. (2008) High-resolution carbon dioxide concentration record
1109 650,000–800,000 years before present. *Nature* **453**, 379.

1110 Macko S. A. and Estep M. F. Microbial alteration of stable nitrogen and carbon isotopic compositions of
1111 organic matter. , 4.

1112 Macko S., Helleur R., Hartley G. and Jackman P. (1990) Diagenesis of organic matter—a study using
1113 stable isotopes of individual carbohydrates. *Org. Geochem.* **16**, 1129–1137.

1114 Martínez-García A., Sigman D. M., Ren H., Anderson R. F., Straub M., Hodell D. A., Jaccard S. L., Eglinton
1115 T. I. and Haug G. H. (2014) Iron fertilization of the Subantarctic Ocean during the last ice age.
1116 *Science* **343**, 1347–1350.

1117 Maslin M., Hall M., Shackleton N. and Thomas E. (1996) Calculating surface water pCO2 from
1118 foraminiferal organic δ13C. *Geochim. Cosmochim. Acta* **60**, 5089–5100.

1119 Maslin M., Thomas E., Shackleton N., Hall M. and Seidov D. (1997) Glacial northeast Atlantic surface
1120 water pCO2: productivity and deep-water formation. *Mar. Geol.* **144**, 177–190.

1121 McConnaughey T. (1989) 13C and 18O isotopic disequilibrium in biological carbonates: I. Patterns.
1122 *Geochim. Cosmochim. Acta* **53**, 151–162.

1123 McCutchan J. H., Lewis W. M., Kendall C. and McGrath C. C. (2003) Variation in trophic shift for stable
1124 isotope ratios of carbon, nitrogen, and sulfur. *Oikos* **102**, 378–390.

1125 Mehra O. P. and Jackson M. L. (2013) Iron Oxide Removl From Soils and Clays By A Dithionite -Citrate
1126 System Buffered With Sdium Bicarbonate. In *Clays and Clay Minerals* (ed. E. INGERSON).
1127 Pergamon. pp. 317–327. Available at:
1128 http://www.sciencedirect.com/science/article/pii/B9780080092355500267.

1129 Mejía L. M., Méndez-Vicente A., Abrevaya L., Lawrence K. T., Ladlow C., Bolton C., Cacho I. and Stoll H.
1130 (2017) A diatom record of CO2 decline since the late Miocene. *Earth Planet. Sci. Lett.* **479**, 18–
1131 33.

1132 Miller A. G., Espie G. S. and Canvin D. T. (1990) Physiological aspects of CO2 and HCO3− transport by
1133 cyanobacteria: a review. *Can. J. Bot.* **68**, 1291–1302.

1134 Mollenhauer G., Eglinton T. I., Ohkouchi N., Schneider R. R., Müller P. J., Grootes P. M. and Rullkötter J.
1135 (2003) Asynchronous alkenone and foraminifera records from the Benguela Upwelling System.
1136 *Geochim. Cosmochim. Acta* **67**, 2157–2171.

1137 Mook W. G. (1986) 13C in atmospheric CO2. *Neth. J. Sea Res.* **20**, 211–223.

1138 Mook W. G., Bommerson J. C. and Staverman W. H. (1974) Carbon isotope fractionation between
1139 dissolved bicarbonate and gaseous carbon dioxide. *Earth Planet. Sci. Lett.* **22**, 169–176.

1140 Murray J. W. (2001) The niche of benthic foraminifera, critical thresholds and proxies. *Mar.*
1141 *Micropaleontol.* **41**, 1–7.

1142 Nakatsuka T., Handa N., Harada N., Sugimoto T. and Imaizumi S. (1997) Origin and decomposition of
1143 sinking particulate organic matter in the deep water column inferred from the vertical
1144 distributions of its δ15N, δ13 and δ14. *Deep Sea Res. Part Oceanogr. Res. Pap.* **44**, 1957–1979.

Ohkouchi N., Eglinton T. I., Keigwin L. D. and Hayes J. M. (2002) Spatial and Temporal Offsets Between Proxy Records in a Sediment Drift. *Science* **298**, 1224.

Pagani M. (2013) *Biomarker-Based Inferences of Past Climate: The Alkenone pCO2 Proxy*.,

Pagani M., Arthur M. A. and Freeman K. H. (1999) Miocene evolution of atmospheric carbon dioxide. *Paleoceanography* **14**, 273–292.

Pagani M., Freeman K. H., Ohkouchi N. and Caldeira K. (2002) Comparison of water column [CO2aq] with sedimentary alkenone-based estimates: A test of the alkenone-CO2 proxy. *Paleoceanogr. Paleoclimatology* **17**.

Patterson M. R., Sebens K. P. and Olson R. R. (1991) In situ measurements of flow effects on primary production and dark respiration in reef corals. *Limnol. Oceanogr.* **36**, 936–948.

Pearson P. N. (2012) Oxygen isotopes in foraminifera: Overview and historical review. *Paleontol. Soc. Pap.* **18**, 1–38.

Pearson P. N. and Palmer M. R. (2000) Atmospheric carbon dioxide concentrations over the past 60 million years. *Nature* **406**, 695–699.

Polissar P. J., Fulton J. M., Junium C. K., Turich C. C. and Freeman K. H. (2009) Measurement of 13C and 15N Isotopic Composition on Nanomolar Quantities of C and N. *Anal. Chem.* **81**, 755–763.

Popp B. N., Kenig F., Wakeham S. G., Laws E. A. and Bidigare R. R. (1998) Does growth rate affect ketone unsaturation and intracellular carbon isotopic variability in Emiliania huxleyi? *Paleoceanography* **13**, 35–41.

Popp B. N., Takigiku R., Hayes J. M., Louda J. W. and Baker E. W. (1989) The post-Paleozoic chronology and mechanism of 13 C depletion in primary marine organic matter. *Am. J. Sci.* **289**, 436–454.

Prahl F. G. and Wakeham S. G. (1987) Calibration of unsaturation patterns in long-chain ketone compositions for palaeotemperature assessment. *Nature* **330**, 367.

Rau G. H., Froelich P. N., Takahashi T. and Marais D. J. D. (1991) Does Sedimentary Organic δ13C Record Variations in Quaternary Ocean [CO2(aq)]? *Paleoceanography* **6**, 335–347.

Rau G. H., Riebesell U. and Wolf-Gladrow D. (1997) CO2aq-dependent photosynthetic 13C fractionation in the ocean: A model versus measurements. *Glob. Biogeochem. Cycles* **11**, 267–278.

Rau G. H., Sweeney R. E. and Kaplan I. R. (1982) Plankton 13C: 12C ratio changes with latitude: differences between northern and southern oceans. *Deep Sea Res. Part Oceanogr. Res. Pap.* **29**, 1035–1039.

Rau G. H., Takahashi T., Des Marais D. J., Repeta D. J. and Martin J. H. (1992) The relationship between δ13C of organic matter and [CO2(aq)] in ocean surface water: Data from a JGOFS site in the northeast Atlantic Ocean and a model. *Geochim. Cosmochim. Acta* **56**, 1413–1419.

1178 Rau G. H., Takahashi T. and Marais D. J. D. (1989) Latitudinal variations in plankton δ13C: implications
1179 for CO2 and productivity in past oceans. *Nature* **341**, 516.

1180 Ren H., Sigman D. M., Martínez-García A., Anderson R. F., Chen M.-T., Ravelo A. C., Straub M., Wong G.
1181 T. and Haug G. H. (2017) Impact of glacial/interglacial sea level change on the ocean nitrogen
1182 cycle. *Proc. Natl. Acad. Sci.* **114**, E6759–E6766.

1183 Ren H., Sigman D. M., Meckler A. N., Plessen B., Robinson R. S., Rosenthal Y. and Haug G. H. (2009)
1184 Foraminiferal Isotope Evidence of Reduced Nitrogen Fixation in the Ice Age Atlantic Ocean.
1185 *Science* **323**, 244.

1186 Ren H., Sigman D. M., Thunell R. C. and Prokopenko M. G. (2012) Nitrogen isotopic composition of
1187 planktonic foraminifera from the modern ocean and recent sediments. *Limnol. Oceanogr.* **57**,
1188 1011–1024.

1189 Ren H., Studer A. S., Serno S., Sigman D. M., Winckler G., Anderson R. F., Oleynik S., Gersonde R. and
1190 Haug G. H. (2015) Glacial-to-interglacial changes in nitrate supply and consumption in the
1191 subarctic North Pacific from microfossil-bound N isotopes at two trophic levels.
1192 *Paleoceanography* **30**, 1217–1232.

1193 Rink S., Kühl M., Bijma J. and Spero H. J. (1998) Microsensor studies of photosynthesis and respiration in
1194 the symbiotic foraminifer Orbulina universa. *Mar. Biol.* **131**, 583–595.

1195 Robbins L. L. and Brew K. (1990) Proteins from the organic matrix of core-top and fossil planktonic
1196 foraminifera. *Geochim. Cosmochim. Acta* **54**, 2285–2292.

1197 Rodger Harvey H., Tuttle J. H. and Tyler Bell J. (1995) Kinetics of phytoplankton decay during simulated
1198 sedimentation: Changes in biochemical composition and microbial activity under oxic and anoxic
1199 conditions. *Geochim. Cosmochim. Acta* **59**, 3367–3377.

1200 Romanek C. S., Grossman E. L. and Morse J. W. (1992) Carbon isotopic fractionation in synthetic
1201 aragonite and calcite: Effects of temperature and precipitation rate. *Geochim. Cosmochim. Acta*
1202 **56**, 419–430.

1203 Royer D. L., Berner R. A., Montañez I. P., Tabor N. J. and Beerling D. J. (2004) Co~ 2 as a primary driver of
1204 phanerozoic climate. *GSA Today* **14**, 4–10.

1205 Ruddiman W. F. (2003) The anthropogenic greenhouse era began thousands of years ago. *Clim. Change*
1206 **61**, 261–293.

1207 Sautter L. R. and Thunell R. C. (1991) Seasonal Variability in the δ18O and δ13C of Planktonic
1208 Foraminifera from an Upwelling Environment: Sediment Trap Results from the San Pedro Basin,
1209 Southern California Bight. *Paleoceanography* **6**, 307–334.

1210 Schiebel R. and Hemleben C. (2017) *Planktic foraminifers in the modern ocean*., Springer.

1211 Schmidt G. (1999) Global seawater oxygen-18 database. *Httpdata Giss Nasa Govo18data*.

Schroeder R. A. (1975) Absence of β-alanine and γ-aminobutyric acid in cleaned foraminiferal shells: implications for use as a chemical criterion to indicate removal of non-indigenous amino acid contaminants. *Earth Planet. Sci. Lett.* **25**, 274–278.

Singer A. J. and Shemesh A. (1995) Climatically linked carbon isotope variation during the past 430,000 years in Southern Ocean sediments. *Paleoceanography* **10**, 171–177.

Smith D., Simon M., L. Alldredge A. and Azam F. (1992) *Intense hydrolytic enzyme activity on marine aggregates and implications for rapid particle dissolution*.,

Spero H. J. (1988) Ultrastructural examination of chamber morphogenesis and biomineralization in the planktonic foraminiferOrbulina universa. *Mar. Biol.* **99**, 9–20.

Spero H. J. and Parker S. L. (1985) Photosynthesis in the symbiotic planktonic foraminifer Orbulina universa, and its potential contribution to oceanic primary productivity. *J. Foraminifer. Res.* **15**, 273–281.

Spindler M., Hemleben C., Salomons J. and Smit L. (1984) Feeding behavior of some planktonic foraminifers in laboratory cultures. *J. Foraminifer. Res.* **14**, 237–249.

Stathoplos L. and Hare P. (1989) Amino acids in planktonic foraminifera: are they phylogenetically useful? In *Origin, Evolution, and Modern Aspects of Biomineralization in Plants and Animals* Springer. pp. 329–338.

Stoll H. M., Guitian J., Hernandez-Almeida I., Mejia L. M., Phelps S., Polissar P., Rosenthal Y., Zhang H. and Ziveri P. (2019) Upregulation of phytoplankton carbon concentrating mechanisms during low CO2 glacial periods and implications for the phytoplankton pCO2 proxy. *Quat. Sci. Rev.* **208**, 1–20.

Stott L. D. (1992) Higher temperatures and lower oceanic pCO2: A climate enigma at the end of the Paleocene Epoch. *Paleoceanography* **7**, 395–404.

Straub M., Sigman D. M., Ren H., Martínez-García A., Meckler A. N., Hain M. P. and Haug G. H. (2013) Changes in North Atlantic nitrogen fixation controlled by ocean circulation. *Nature* **501**, 200.

Sunda W. G. and Huntsman S. A. (1997) Interrelated influence of iron, light and cell size on marine phytoplankton growth. *Nature* **390**, 389.

Swart P. K. (1983) Carbon and oxygen isotope fractionation in scleractinian corals: a review. *Earth-Sci. Rev.* **19**, 51–80.

Swart P. K., Saied A. and Lamb K. (2005) Temporal and spatial variation in the δ15N and δ13C of coral tissue and zooxanthellae in Montastraea faveolata collected from the Florida reef tract. *Limnol. Oceanogr.* **50**, 1049–1058.

T Marlowe I., Green J. C., Neal A. C., Brassell S., Eglinton G. and Course P. A. (1984) *Long chain (n-C37-C39) alkenones in the Prymnesiophycea. Distribution of alkenones and other lipids and their taxonomic significance*.,

1247 Taylor K. E., Stouffer R. J. and Meehl G. A. (2012) An overview of CMIP5 and the experiment design. *Bull.*
1248 *Am. Meteorol. Soc.* **93**, 485–498.

1249 Uhle M. E., Macko S. A., Spero H. J., Engel M. H. and Lea D. W. (1997) Sources of carbon and nitrogen in
1250 modern planktonic foraminifera: the role of algal symbionts as determined by bulk and
1251 compound specific stable isotopic analyses. *Org. Geochem. Paleoclimatic Markers Prod. Preserv.*
1252 *Model.* **27**, 103–113.

1253 Werdell P. J., Franz B. A., Bailey S. W., Feldman G. C., Boss E., Brando V. E., Dowell M., Hirata T.,
1254 Lavender S. J. and Lee Z. (2013) Generalized ocean color inversion model for retrieving marine
1255 inherent optical properties. *Appl. Opt.* **52**, 2019–2037.

1256 Wilkes E. B. and Pearson A. (2019) A general model for carbon isotopes in red-lineage phytoplankton:
1257 Interplay between unidirectional processes and fractionation by RubisCO. *Geochim. Cosmochim.*
1258 *Acta* **265**, 163–181.

1259 Wolf-Gladrow D. A., Bijma J. and Zeebe R. E. (1999) Model simulation of the carbonate chemistry in the
1260 microenvironment of symbiont bearing foraminifera. *Mar. Chem.* **64**, 181–198.

1261 Wooller M., Wang Y. and Axford Y. (2008) A multiple stable isotope record of Late Quaternary
1262 limnological changes and chironomid paleoecology from northeastern Iceland. *J. Paleolimnol.*
1263 **40**, 63–77.

1264 Yan Y., Bender M. L., Brook E. J., Clifford H. M., Kemeny P. C., Kurbatov A. V., Mackay S., Mayewski P. A.,
1265 Ng J. and Severinghaus J. P. (2019) Two-million-year-old snapshots of atmospheric gases from
1266 Antarctic ice. *Nature* **574**, 663–666.

1267 Yoshioka T. (1997) Phytoplanktonic carbon isotope fractionation: equations accounting for CO2-
1268 concentrating mechanisms. *J. Plankton Res.* **19**, 1455–1476.

1269 Zachos J. C., Dickens G. R. and Zeebe R. E. (2008) An early Cenozoic perspective on greenhouse warming
1270 and carbon-cycle dynamics. *Nature* **451**, 279.

1271 Zalasiewicz J., Williams M., Smith A., Barry T. L., Coe A. L., Bown P. R., Brenchley P., Cantrill D., Gale A.
1272 and Gibbard P. (2008) Are we now living in the Anthropocene? *Gsa Today* **18**, 4.

1273 Zanden M. J. V. and Rasmussen J. B. (2001) Variation in δ15N and δ13C trophic fractionation:
1274 Implications for aquatic food web studies. *Limnol. Oceanogr.* **46**, 2061–2066.

1275 Zeebe R. E. (1999) An explanation of the effect of seawater carbonate concentration on foraminiferal
1276 oxygen isotopes. *Geochim. Cosmochim. Acta* **63**, 2001–2007.

1277 Zeebe R. E. and Wolf-Gladrow D. (2001) *CO2 in seawater: equilibrium, kinetics, isotopes*., Gulf
1278 Professional Publishing.

1279 Zhang J., Quay P. and Wilbur D. (1995) Carbon isotope fractionation during gas-water exchange and
1280 dissolution of CO2. *Geochim. Cosmochim. Acta* **59**, 107–114.

1281

Fig. 1. Conceptual model of carbon fluxes within a symbiont-bearing foraminifera (using the spherical morphology of *O. universa*), including key isotopic compositions and fractionations. The fluxes of dissolved inorganic carbon are shown in purple, and the fluxes of organic carbon are in green. Carbon fixation occurs within symbiotic dinoflagellates (shown enlarged, left). Of the chemical species that compose dissolved inorganic carbon, two interact with the dinoflagellate. CO2 diffuses passively into and out of the cell depending on the ratio of the internal and external CO2 concentrations. HCO3− is taken up actively. Interconversion between the two species is facilitated by the enzyme carbonic anhydrase (CA). The isotope effects associated with key carbon fluxes and transformations leading to photosynthetic carbon fixation are shown and enter into discussion in the main text (Section 4.3). The inorganic carbon species isotopic compositions are taken from Keller and Morel (1999). εt is the isotope effect associated with diffusion (Laws et al., 1995), εa with active transport (Yoshioka 1997), and εf with fixation (Rau et al., 1997). εHCO3-/CO2 refers to the temperature-dependent equilibrium isotope effect between HCO3− and aqueous CO2 (equal to 9.866*103/T + 24.12‰, T in °C; Mook et al., 1974). The symbiont is hosted within the foraminifera 'holobiont' (right), where it shows diel motion from within the foraminifera to outside the test (black double-headed arrows). The combination of the symbiont- and feeding-derived organic carbon is used to produce the bulk tissue and the foraminifera-bound organic matter (FBOM). (For interpretation of the references to color in this figure legend, the reader is referred to the web version of this article.)

Fig. 2. Protocol for FBOM-δ13C analysis prior to mass spectrometry. For description of sample preparation (steps 1–3), see Section 2.2. For description of instrument operation (boxes 4, 5), see Section 2.1 (Fig. 3).

Fig. 3. High-sensitivity Dumas combustion-based system for carbon isotopic analysis, adapted from Polissar et al. (2009). The design is divided into 3 parts: a combustion system that consists of a modified Costech elemental analyzer, a cryofocus, and an open split system (i.e., a modified Finnigan Gasbench II) that serves as an interface for a Thermo Delta V Advantage mass spectrometer. The sample is introduced to the system by a modified Costech 'Zero-Blank' autosampler (not shown) and is combusted in a helium stream. Illustrated are 2 custom-built, double-walled reactors for oxidation and reduction furnaces which bifurcate the helium flow into sample and 'sheath' flows (thick and thin red arrows respectively). The sample flow contains the sample, while the sheath flow absorbs atmospheric contamination. As in Polissar et al. (2009), the system enhances sensitivity by freezing the analyte in liquid nitrogen and then directing it to the mass spectrometer under low helium flow. The two operational modes of the cryofocus and open split systems are also shown, with the short-dashed red flow lines indicating lower flow rate. (For interpretation of the references to color in this figure legend, the reader is referred to the web version of this article.)

Fig. 4. Depth profile comparing measured mixed-species foraminiferal carbonate δ18O with co-occurring empirically derived species calibrations (Bemis et al., 1998) given local seawater δ18O (Schmidt, 1999) and the mean modeled temperature profile in the region (taken from CMIP5 NOAA GFDL-CM2.1) (Taylor et al., 2012). The mean value of the mixed-species foraminiferal carbonate δ18O measurements from the region is shown by the black circle, and the range of measured values is shown with horizontal brackets (excluding one outlier, indicated by the asterisk). Mean values of *O. universa* (in both high and low light conditions) and *G. sacculifer* calibrations are shown in the colored lines, with their ranges indicated by brackets. The double-

headed arrows to the right indicate the literature-derived likely depth ranges of the measured species (Emiliani 1971; Faul et al., 2000; Farmer et al., 2007). The gray shading indicates the depth of habitat for the principal species in the mixed species fraction by mass (*G. menardii* and *O. universa*) that allows the predicted mixed-species foraminiferal carbonate δ18O to match the measured values. See supplementary Fig. A1 for comparison among sample sites. (For interpretation of the references to color in this figure legend, the reader is referred to the web version of this article.)

Fig. 5. Surface sediment FBOM-δ13C across the equatorial Pacific and its relationship to upper water column characteristics. (A) Left axis: calculated surface water [CO2(aq)] (pink triangles) from the Surface Ocean CO2 Atlas (SOCAT) (Bakker et al., 2016). Right axis: surface nitrate concentration (orange triangles) from World Ocean Atlas 2018 (Garcia et al., 2019). (B) δ13CCO2 calculated from co-occurring foraminiferal carbonate δ13C ((Mook, 1986; Zhang et al., 1995); Eq. (6), Section 3.2 of text). C) FBOM-δ13C in core top samples from the eastern equatorial Pacific (85.3–110.8°W; see Fig. 6). Species are measured based on availability in the sediment. All data have a precision of 0.4 ‰ (1SD) or better. (D) εFBOM-CO2, derived from (B), (C), and Eq. (7). (For interpretation of the references to color in this figure legend, the reader is referred to the web version of this article.)

Fig. 6. Map of sample sites, with εFBOM-CO2 (markers) as the right color bar and the SOCAT-derived surface [CO2(aq)] (colormap) as the left color bar. Given the directionality and range of the color scales, a strong correlation between [CO2(aq)] and εFBOM-CO2, the colors of the variables should have similar patterns. Also plotted are temperature isolines in °C (taken from CMIP5 NOAA GFDL-CM2.1) (Taylor et al., 2012). See supplementary Fig. A.2 for picked species data. (For interpretation of the references to color in this figure legend, the reader is referred to the web version of this article.)

Fig. 7. Comparison of FBOM-δ13C and εFBOM-CO2 with estimated [CO2(aq)] in the surface waters across all sample sites. FBOM-δ13C and εFBOM-CO2 are shown in the top and bottom rows, respectively: (A, D) mixed species assemblage, (B, E) symbiotic, spinose, euphotic-zone-dwelling species, and (C, F) non-spinose, non-euphotic zone dwelling species. See Table 2 for R-values and slopes of best fit.

Fig. 8. Analysis of the role of phytoplankton growth rate on εFBOM-CO2. For mixed species (A, C; in black filled circles) and *G. menardii* (B, D; in red filled circles), εFBOM-CO2 is plotted against 1/[CO2(aq)] (A, B) and μ/[CO2(aq)] (C,D). 1/[CO2(aq)] is also plotted against μ/[CO2(aq)] (E, F). (For interpretation of the references to color in this figure legend, the reader is referred to the web version of this article.)

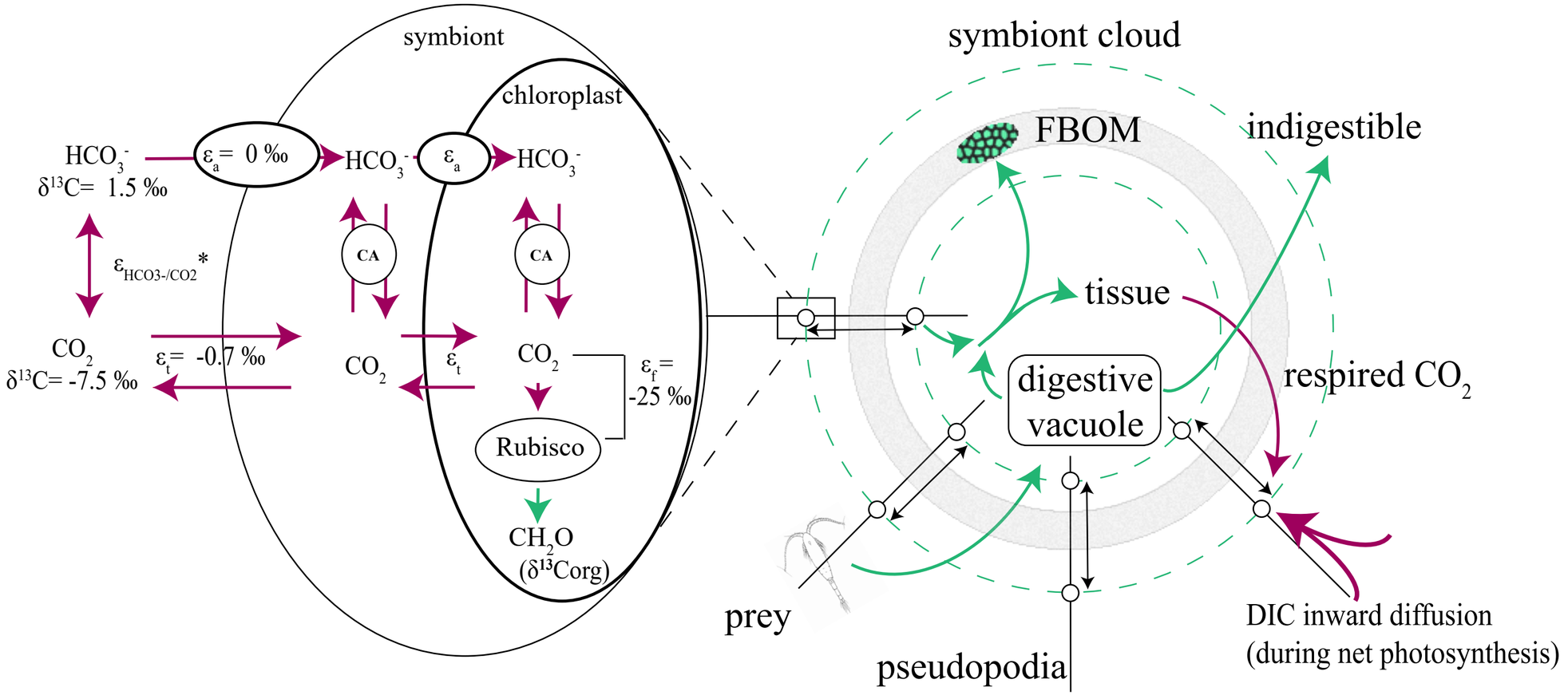
symbiont
chloroplast
HCO3-
δ13C= 1.5 ‰
εa = 0 ‰
HCO3-
εa
HCO3-
εHCO3-/CO2*
CA
CA
CO2
δ13C= -7.5 ‰
εt = -0.7 ‰
CO2
εt
CO2
εf = -25 ‰
Rubisco
CH2O
(δ13Corg)
symbiont cloud
FBOM
indigestible
tissue
digestive vacuole
respired CO2
prey
pseudopodia
DIC inward diffusion
(during net photosynthesis)

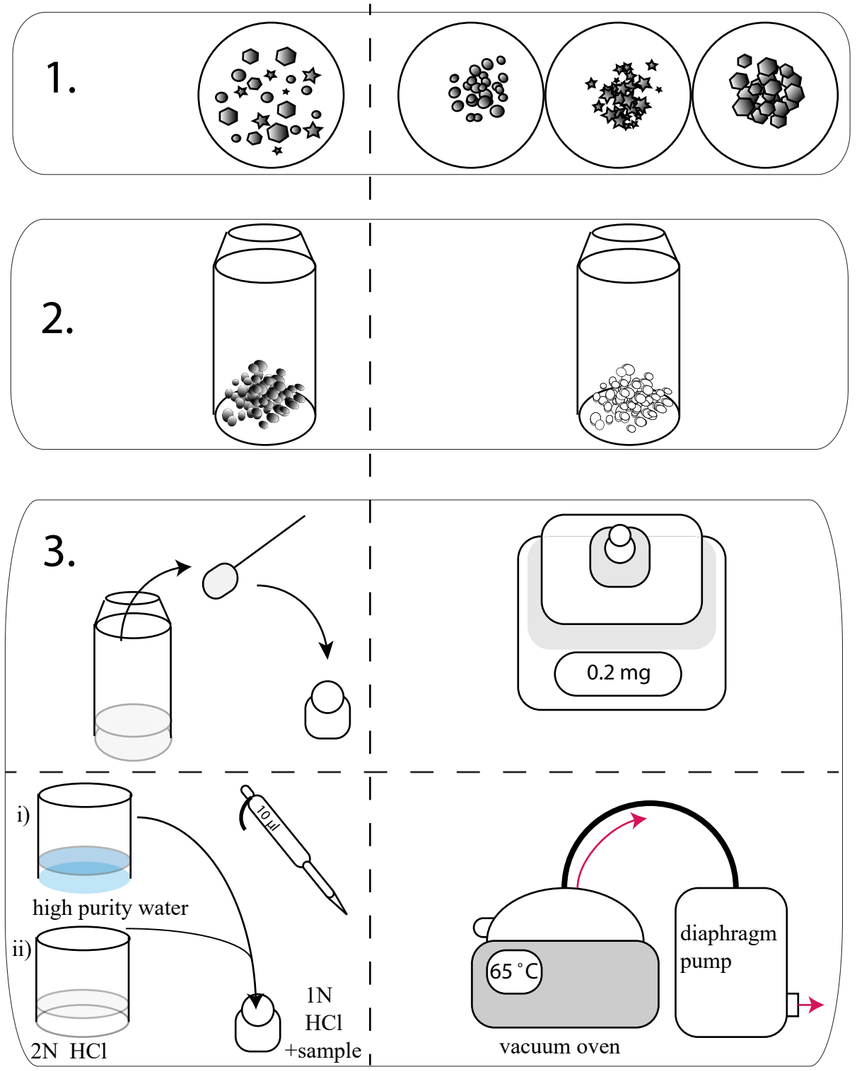

1. sorting

sieve, pick, crack open

2. cleaning

ultrasonicate, rinse, reductive cleaning reagent, rinse, persulfate oxidative reagent, autoclave, rinse, dry

3. decarbonation

pulverize, weigh, acidify, dry , reacidify, redry

4. online combustion:

combust, reduce, remove water

5. cryofocus:

freeze analyte, direct to open split under low helium flow

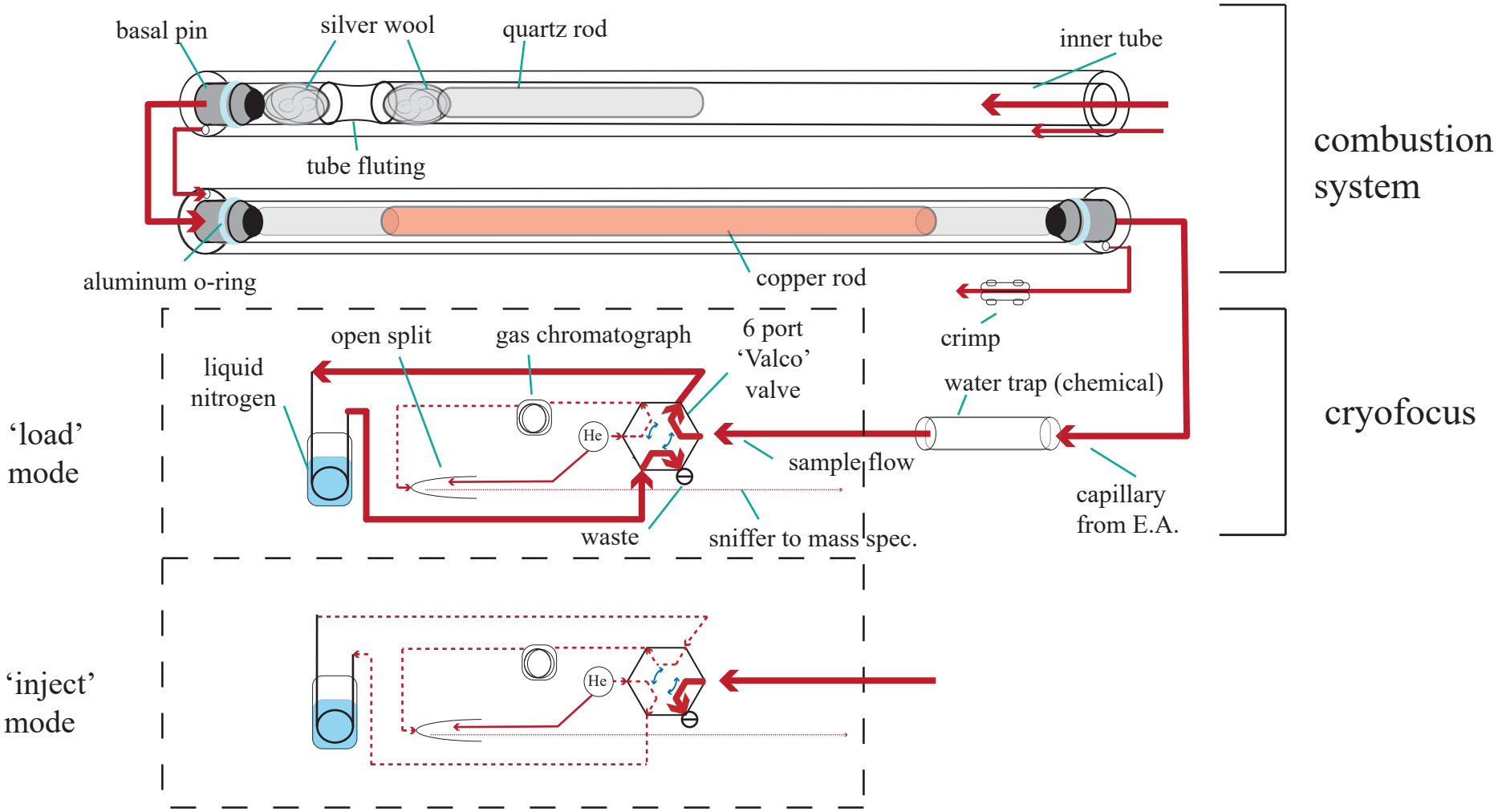
basal pin
silver wool
quartz rod
inner tube
tube fluting
combustion system
aluminum o-ring
copper rod
crimp
cryofocus
'load' mode
open split
gas chromatograph
6 port 'Valco' valve
liquid nitrogen
water trap (chemical)
He
sample flow
capillary from E.A.
waste
sniffer to mass spec.
'inject' mode
He

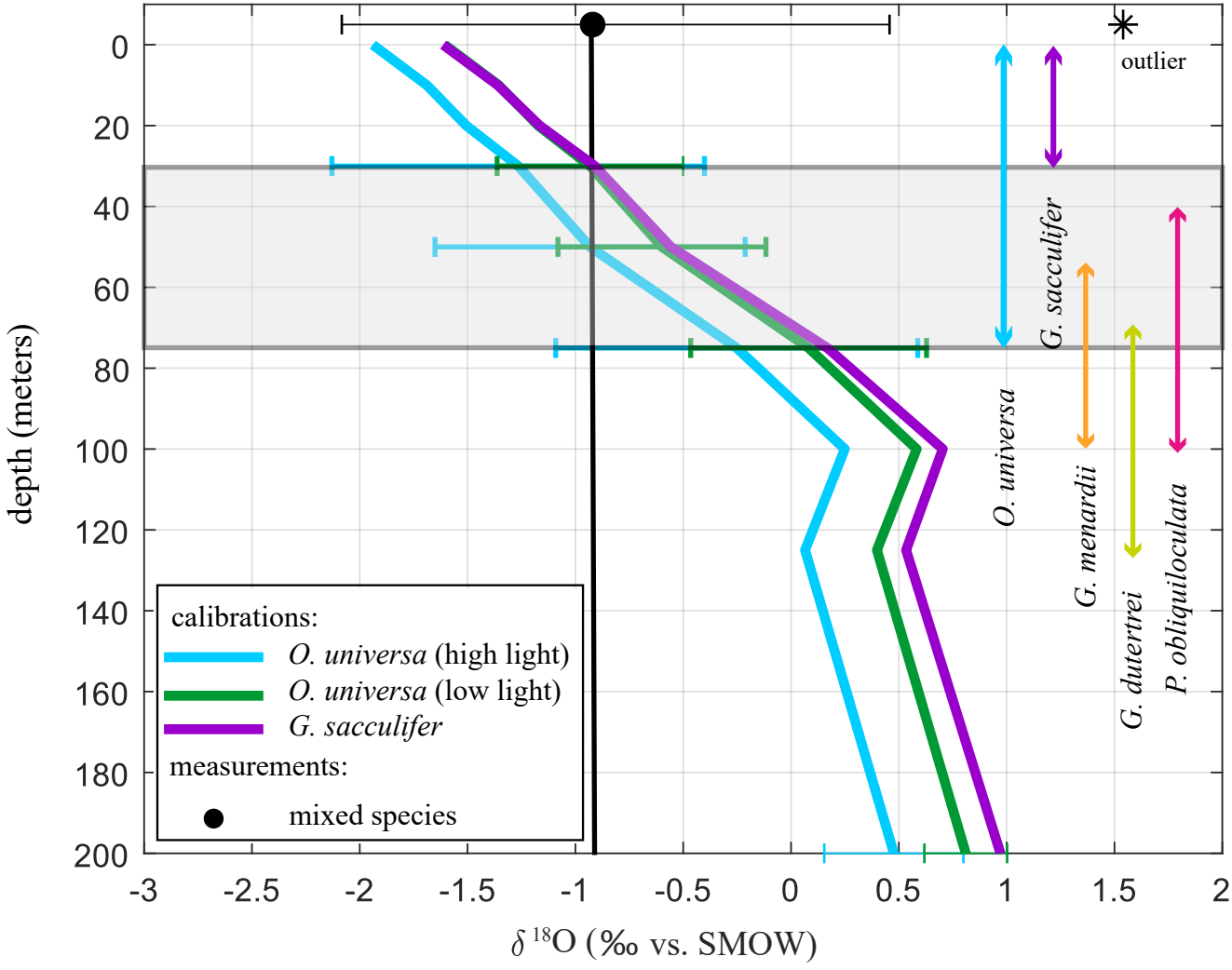
depth (meters)
0
20
40
60
80
100
120
140
160
180
200
-3
-2.5
-2
-1.5
-1
-0.5
0
0.5
1
1.5
2
δ 18O (‰ vs. SMOW)
outlier
O. universa
G. sacculifer
G. menardii
G. dutertrei
P. obliquiloculata
calibrations:
O. universa (high light)
O. universa (low light)
G. sacculifer
measurements:
mixed species

A

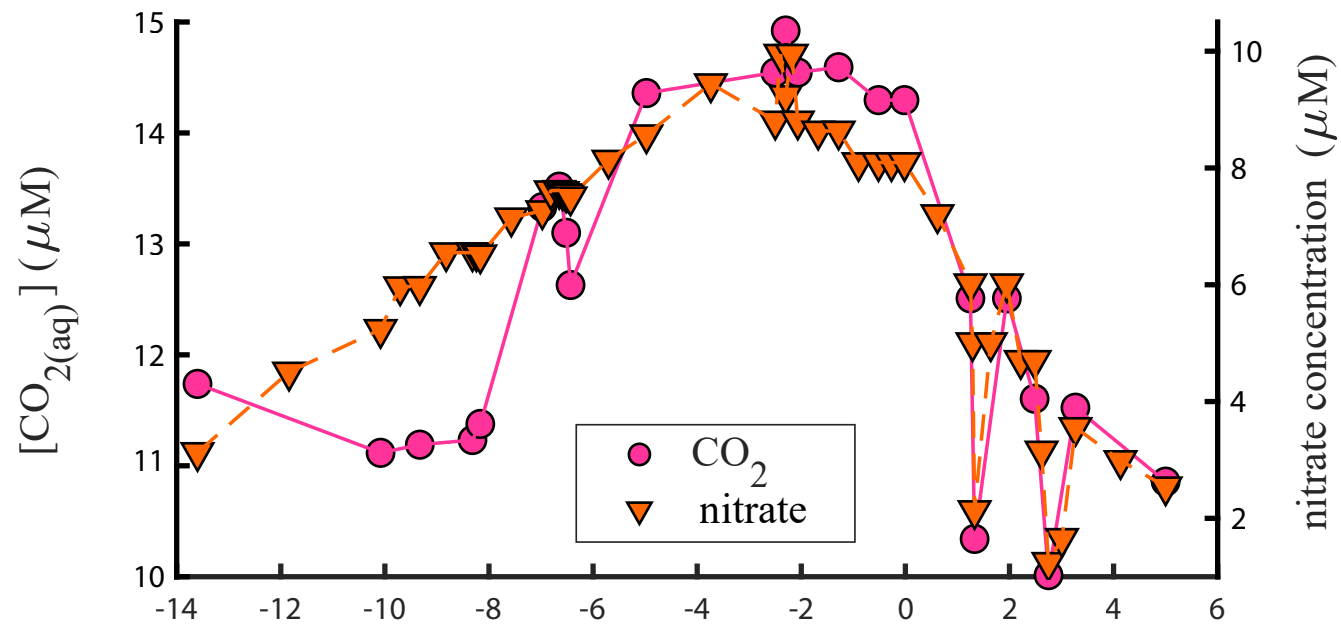

B

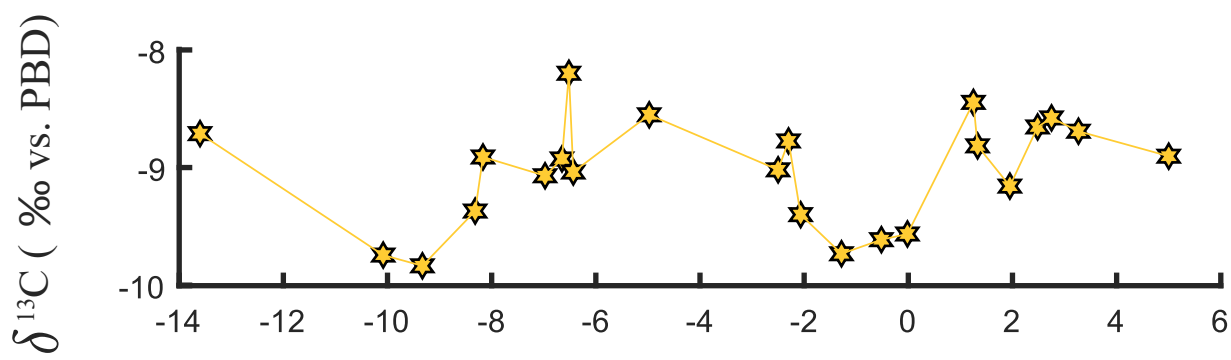

C

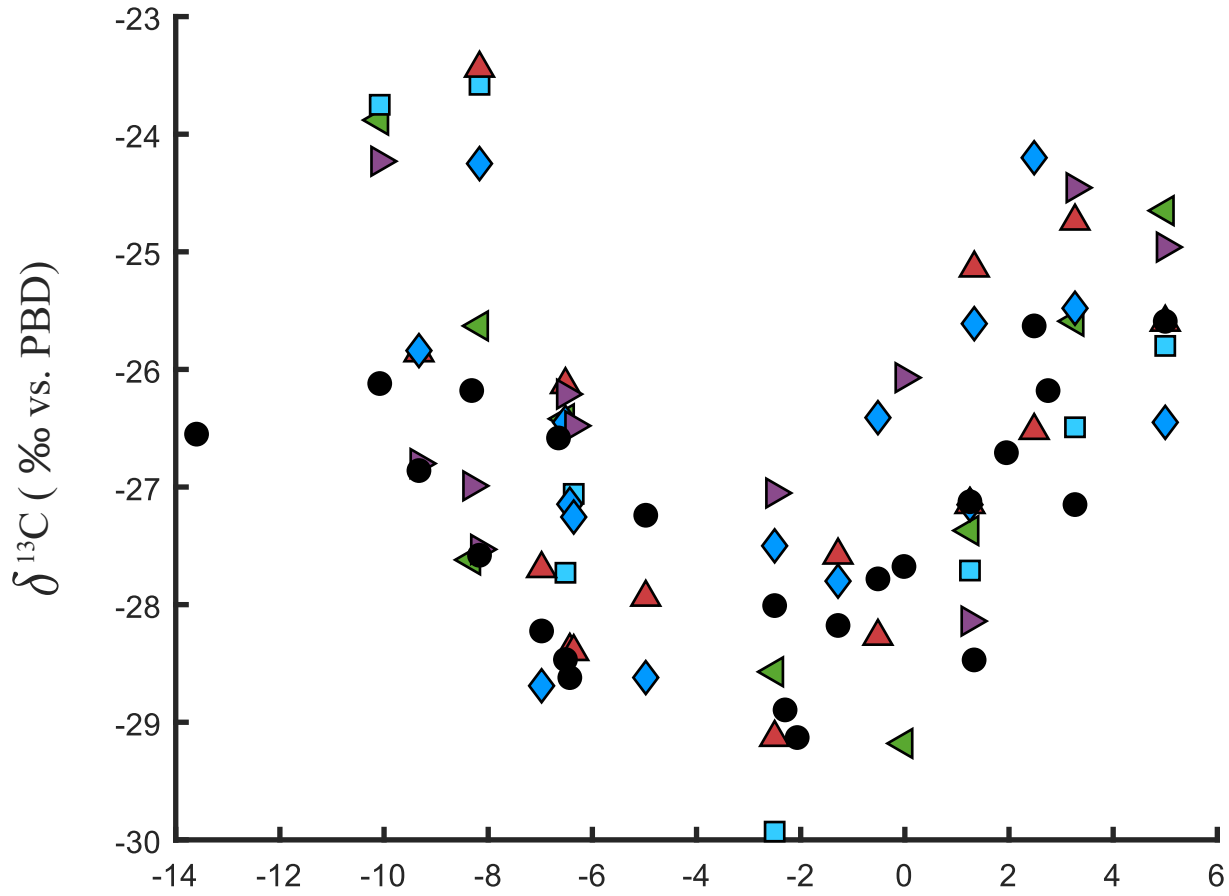

D

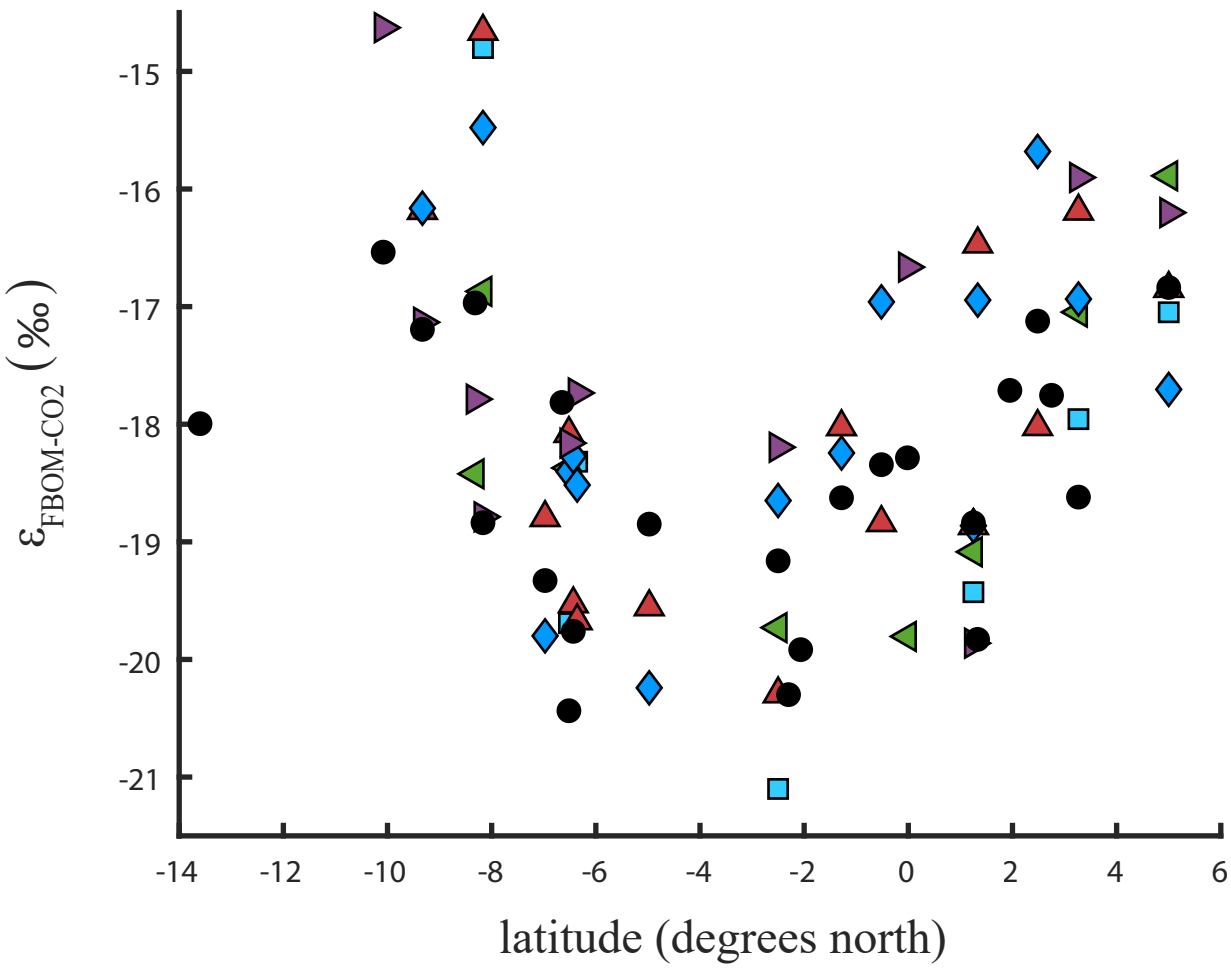

O. universa *G. menardii* *P. obliquiloculata*
G. sacculifer *G. dutertrei* Mixed species

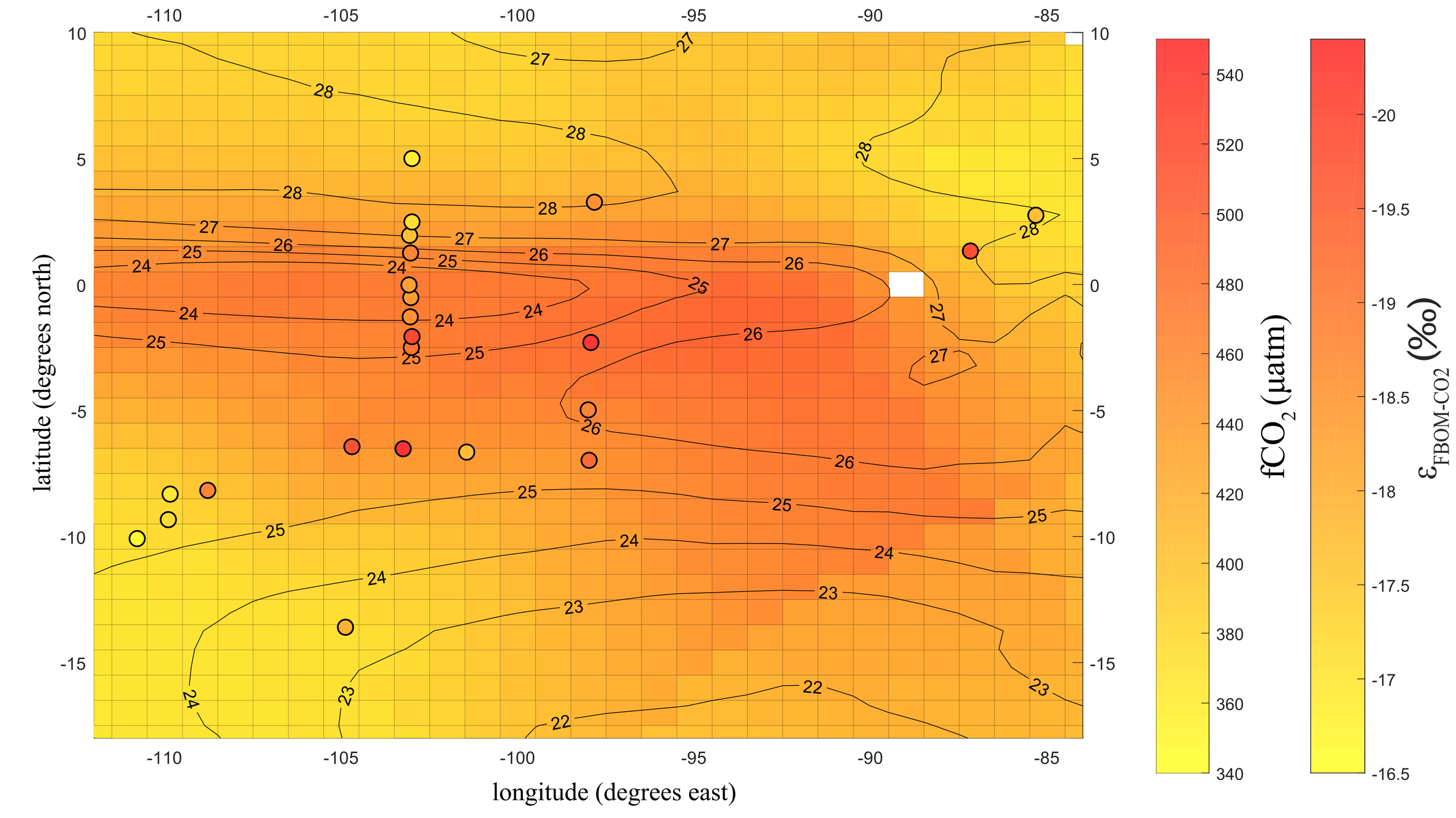
-110
-105
-100
-95
-90
-85
10
5
0
-5
-10
-15
latitude (degrees north)
longitude (degrees east)
fCO2 (µatm)
εFBOM-CO2 (‰)
340
360
380
400
420
440
460
480
500
520
540
-16.5
-17
-17.5
-18
-18.5
-19
-19.5
-20

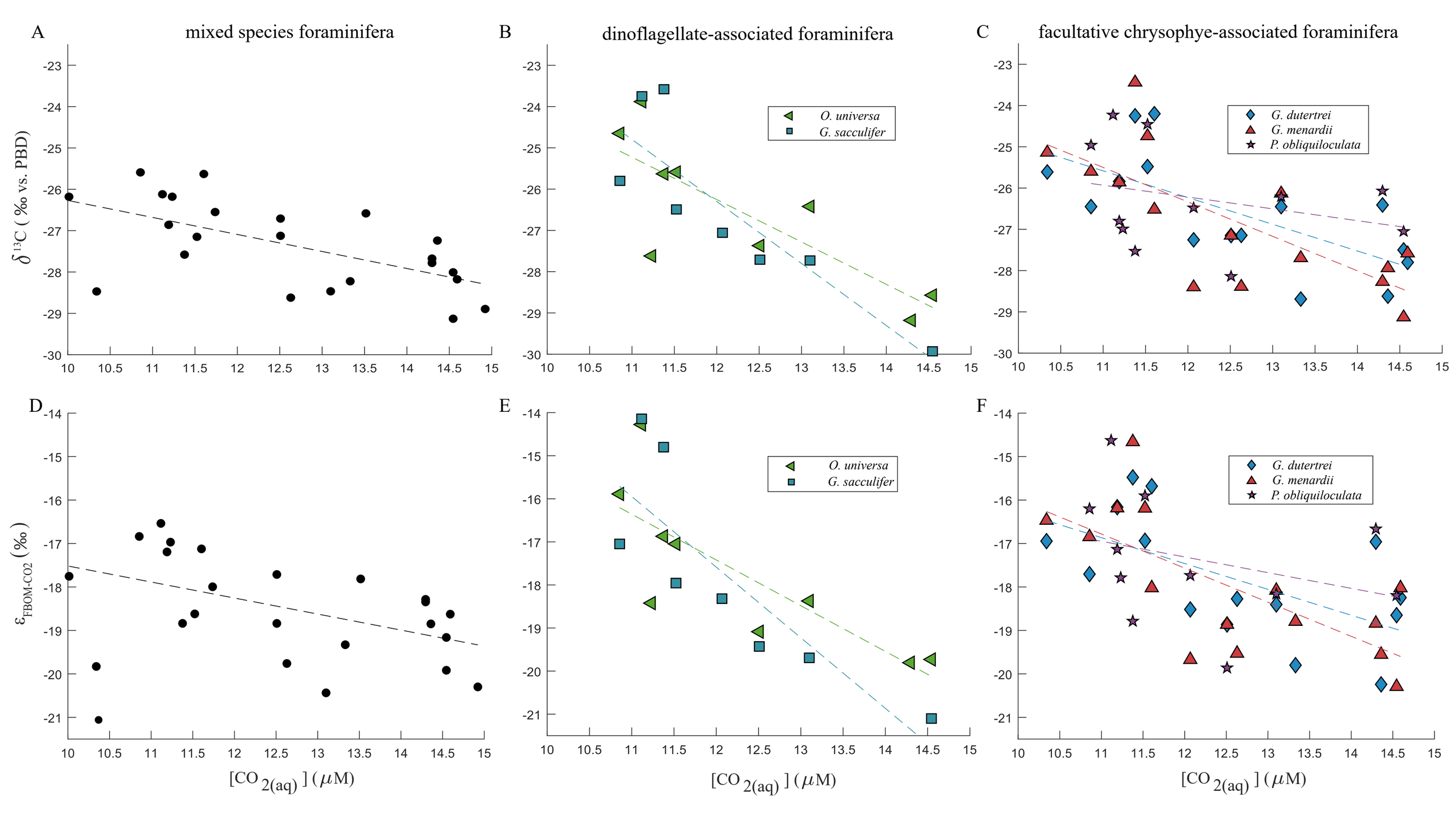
A
mixed species foraminifera
B
dinoflagellate-associated foraminifera
C
facultative chrysophye-associated foraminifera
D
E
F
δ13C (‰ vs. PBD)
εFBOM-CO2 (‰)
[CO2(aq)] (μM)
O. universa
G. sacculifer
G. dutertrei
G. menardii
P. obliquiloculata

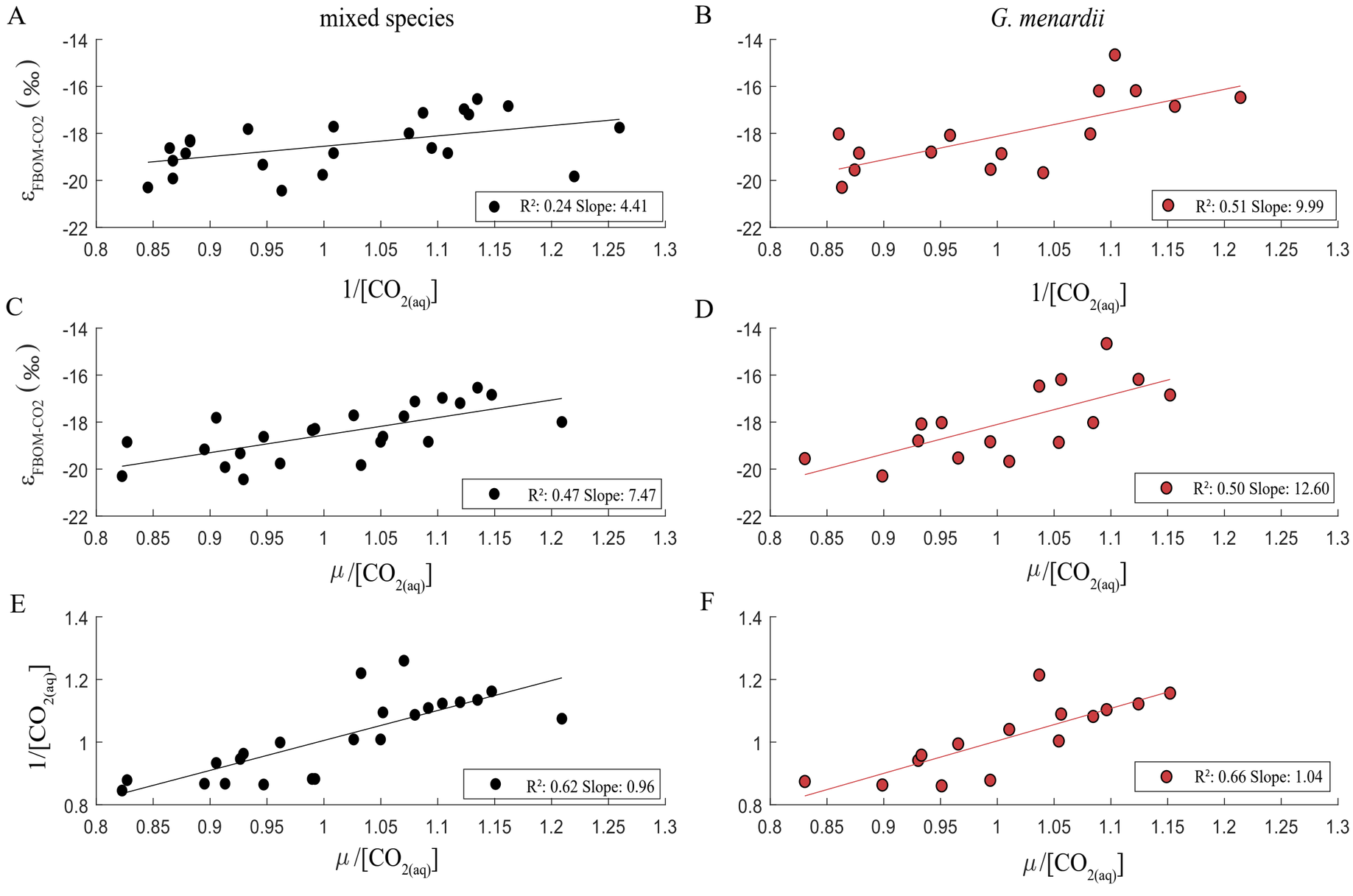
A
mixed species
B
G. menardii
C
D
E
F
$\varepsilon_{FBOM-CO2}$ (‰)
1/[$CO_{2(aq)}$]
μ/[$CO_{2(aq)}$]
R²: 0.24 Slope: 4.41
R²: 0.51 Slope: 9.99
R²: 0.47 Slope: 7.47
R²: 0.50 Slope: 12.60
R²: 0.62 Slope: 0.96
R²: 0.66 Slope: 1.04

Table 1. FBOM carbon isotopic composition and its regression on $[CO_{2(aq)}]$

	Organism	Number of Sites	Mean	Range	Versus $[CO_{2(aq)}]$			Versus $\mu/[CO_{2(aq)}]$			Symbiont Relationship/Identity
					Slope	Correlation Coefficient (R)	Significance	Slope	Correlation Coefficient (R)	Significance	
ε FBOM-$CO_{2(aq)}$	Mixed Species	23	-18.48 (-18.21*)	3.89	-0.37	0.5	Yes ($P < .05$)	7.47	0.69	Very High ($P < .001$)	----------
	G. sacculifer	8	-17.81	6.95	-1.64	0.84	High ($P < .01$)	22.64	0.83	High ($P < .01$)	Obligate Dinoflagellate
	O. universa	9	-17.72	5.53	-1.06	0.80	High ($P < .01$)	16.14	0.74	Yes ($P < .05$)	Obligate Dinoflagellate
	G. menardii	15	-18.00	5.63	-0.78	0.69	High ($P < .01$)	12.60	0.71	High ($P < .01$)	Facultative Chrysophyte
	G. dutertrei	15	-17.79	4.49	-0.60	0.60	Yes ($P < .05$	11.86	0.75	Very High ($P < .001$)	Facultative Chrysophyte
	P. obliquiloculata	11	-17.37	5.23	-0.36	0.32	No ($P < .05$)	6.68	0.39	No ($P < .05$)	Facultative Chrysophyte

	Organism	Number of Sites	Mean	Range	Versus $[CO_{2(aq)}]$			Versus $\mu/[CO_{2(aq)}]$			Symbiont Relationship/Identity
					Slope	Correlation Coefficient (R)	Significance	Slope	Correlation Coefficient (R)	Significance	
$\delta^{13}C$	Mixed Species	23	-27.35	3.54	-0.41	0.61	High ($P < .01$)	6.84	0.68	Very High ($P < .001$)	----------
	G. sacculifer	8	-26.43	6.35	-1.5	0.87	High ($P < .01$)	20.1	0.83	High ($P < .01$)	Obligate Dinoflagellate
	O. universa	9	-26.55	5.30	-1.03	0.81	High ($P < .01$)	13.89	0.69	Yes ($P < .05$)	Obligate Dinoflagellate
	G. menardii	15	-26.80	5.69	-0.84	0.73	High ($P < .01$)	11.77	0.65	High ($P < .01$)	Facultative Chrysophyte
	G. dutertrei	15	-26.59	4.49	-0.65	0.68	High ($P < .01$)	11.04	0.73	Very High ($P < .001$)	Facultative Chrysophyte
	P. obliquiloculata	11	-26.24	3.91	-0.28	0.30	No ($P < .05$)	3.71	0.24	No ($P < .05$)	Facultative Chrysophyte

Corrected for Contaminants (See Section 4.4.4.)

Table 2. Core description and inorganic isotopic metadata

Cruise	Core	Mean $\delta^{13}C$ (‰ vs. PBD)	Mean $\delta^{18}O$ (‰ vs. PBD	Latitude (degrees north)	Longitude (degrees east)	Water Depth (meters)	Regional Sedimentation Rate (cm/kyr)
P6702	024-03	1.13	0.05	-13.60	-104.88	3983	1.8
P6702	030-03	-0.10	-2.08	-10.08	-110.78	3295	1.8
P6702	034-03	-0.20	-0.51	-9.33	-109.90	2807	1.8
P6702	035-03	0.23	-2.07	-8.32	-109.85	2914	1.8
P6702	037-03	0.71	-1.12	-8.17	-108.78	3268	1.8
GS7202	019-03	0.66	-0.73	-6.98	-97.98	3842	3.1
P6702	048-03	0.83	-1.48	-6.65	-101.45	4209	5.1
P6702	047-03	1.57	1.54	-6.57	-103.25	3780	5.1
P6702	046-03	0.69	-1.03	-6.43	-104.70	3802	5.1
GS7202	018-03	1.28	0.46	-4.98	-98.02	3869	3.1
P6702	010-02	0.91	-0.17	-2.50	-103.02	3101	2.4
GS7202	017-02	1.15	-0.84	-2.30	-97.93	3371	3.1
P6702	009-03	0.53	-1.41	-2.07	-103	3281	2.4
P6702	008-03	0.24	-0.80	-1.28	-103.05	3353	2.4
P6702	004-03	1.22	-0.46	-1.25	-103.04	3317	2.4
P6702	058-03	0.85	-1.59	-1.33	-87.20	2758	5.4
P6702	002-02	0.84	-1.23	-2.48	-103	3354	2.4
P6702	007-03	0.35	-0.82	-0.52	-103.03	3315	2.4
P6702	006-02	0.40	-0.69	-0.02	-103.08	3353	2.4
P6702	003-03	0.51	-0.61	1.95	-103.07	3275	2.4
P6702	059-02	0.88	-1.17	2.75	-85.33	3274	5.4
GS7202	015-02	0.74	-0.54	3.27	-97.83	2986	3.1
P6702	001-02	0.55	-1.41	5.00	-103	3159	2.4

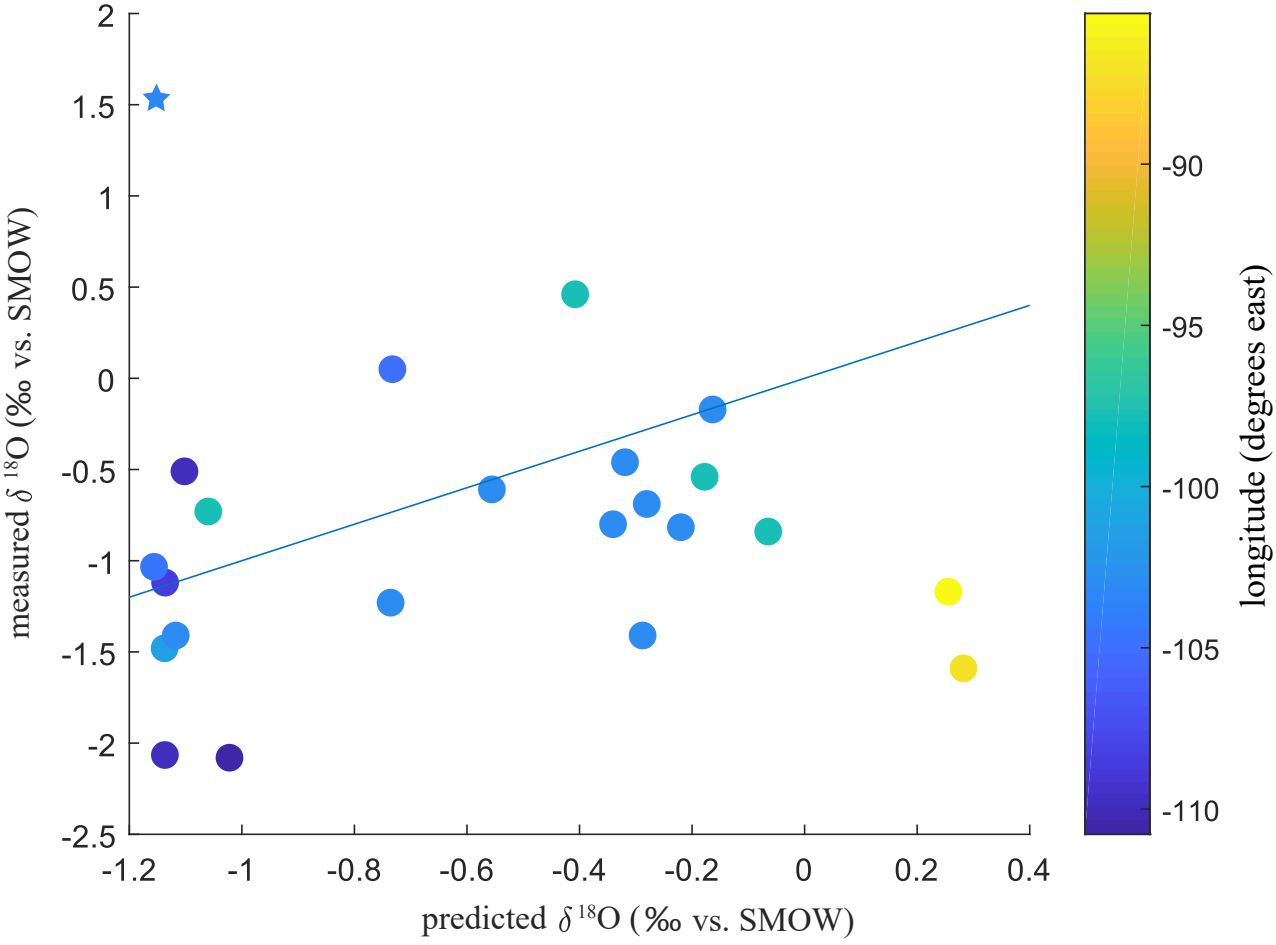

Fig. A.1. Crossplot of measured mixed-species foraminiferal carbonate $\delta^{18}O$ and predicted cooccurring low-light condition *O. universa* $\delta^{18}O$, assuming 50 m depth and empirically derived species calibrations (as in Fig. 4) (Bemis et al., 1998). The color bar indicates the longitude of the core top location and the plotted line is 1:1.

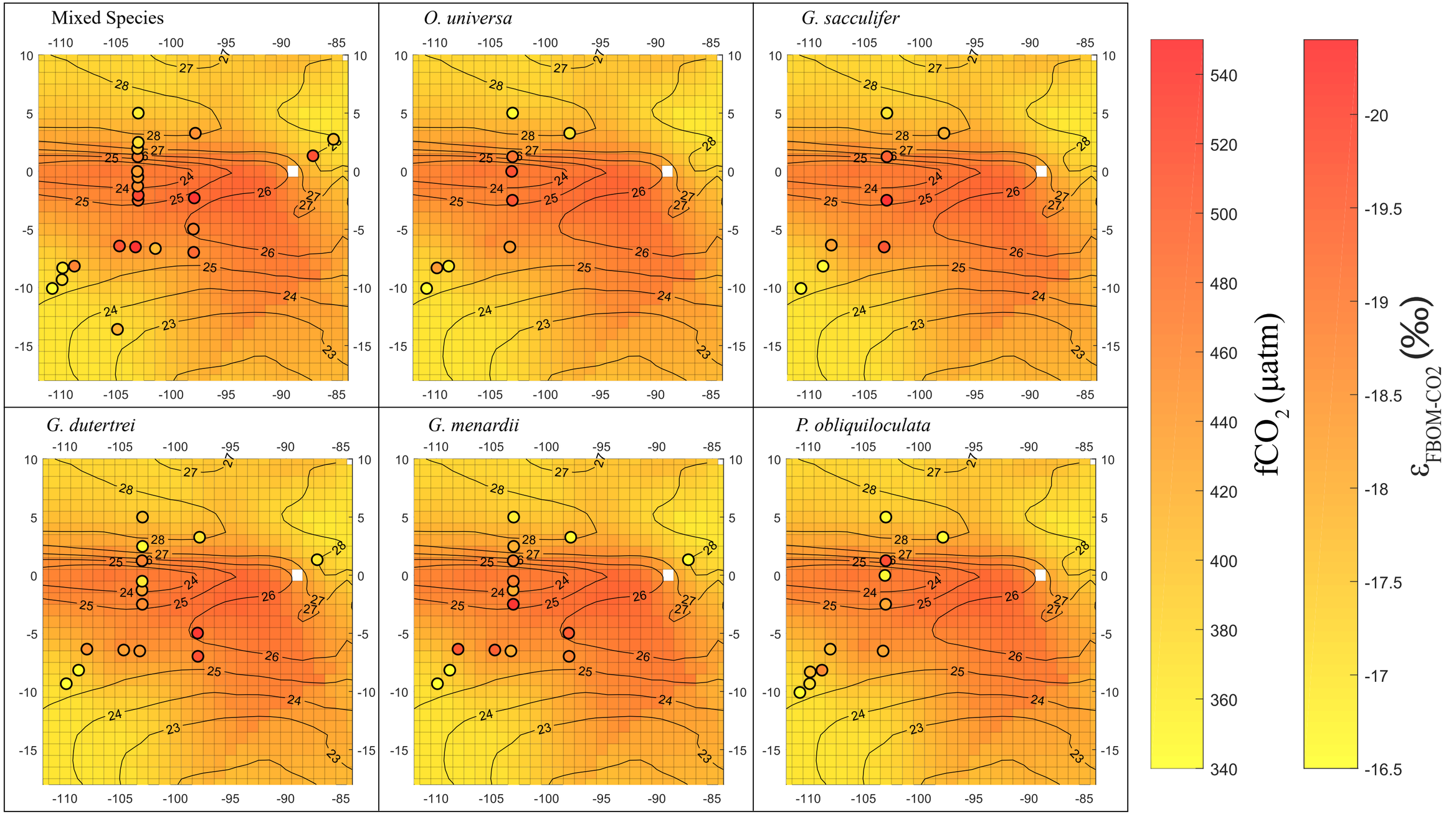

Fig. A.2. As in Fig. 6, but including picked species analyses. $\varepsilon_{FBOM\text{-}CO2}$ (markers) is the right color bar and the SOCAT-derived surface $[CO_{2(aq)}]$ (shading) is the left color bar.